



University of Kentucky  
UKnowledge

---

University of Kentucky Master's Theses

Graduate School

---

2006

## RELATIVE ENERGY CALIBRATION OF THE TJNAF HALL-B PHOTON TAGGER AND INVESTIGATION OF LIMITATIONS OF THE PHOTON TAGGING TECHNIQUE

Marianna Gabrielyan  
*University of Kentucky*, [gab\\_mar27@yahoo.com](mailto:gab_mar27@yahoo.com)

[Right click to open a feedback form in a new tab to let us know how this document benefits you.](#)

---

### Recommended Citation

Gabrielyan, Marianna, "RELATIVE ENERGY CALIBRATION OF THE TJNAF HALL-B PHOTON TAGGER AND INVESTIGATION OF LIMITATIONS OF THE PHOTON TAGGING TECHNIQUE" (2006). *University of Kentucky Master's Theses*. 405.  
[https://uknowledge.uky.edu/gradschool\\_theses/405](https://uknowledge.uky.edu/gradschool_theses/405)

This Thesis is brought to you for free and open access by the Graduate School at UKnowledge. It has been accepted for inclusion in University of Kentucky Master's Theses by an authorized administrator of UKnowledge. For more information, please contact [UKnowledge@lsv.uky.edu](mailto:UKnowledge@lsv.uky.edu).

## ABSTRACT OF THESIS

### RELATIVE ENERGY CALIBRATION OF THE TJNAF HALL-B PHOTON TAGGER AND INVESTIGATION OF LIMITATIONS OF THE PHOTON TAGGING TECHNIQUE

In this work we report on two sets of measurements involving the Hall-B photon tagging system of the Thomas Jefferson National Accelerator Facility. The relative energy calibration of the tagging counters was performed by using the PrimEx pair spectrometer and a series of high position resolution micro-strip detectors. The photon energies were determined by forming coincidence between the tagger and the  $e^+ e^-$  pairs for several values of the pair spectrometer magnetic field between 0.36T to 1.9T (total of 180 fields). The second set of measurements, collected in conjunction with the Fall 2004 PrimEx run, investigated inherent limitations on the photon tagging technique. We report for the first time an experimental signature for these effects.

**KEYWORDS:** Photon tagger, Micro-strip detector, Pair spectrometer, Bremsstrahlung tagging technique, Limitations of the tagging technique.

Marianna Gabrielyan

Author

July 28, 2006

Date

RELATIVE ENERGY CALIBRATION OF THE TJNAF HALL-B PHOTON TAGGER AND  
INVESTIGATION OF LIMITATIONS OF THE PHOTON TAGGING TECHNIQUE

By

Marianna Gabrielyan

Dr. Daniel Dale

Director of Thesis

Dr. Thomas Troland

Director of Graduate Studies

July 28, 2006

Date



THESIS

Marianna Y. Gabrielyan

The Graduate School

University of Kentucky

2006

RELATIVE ENERGY CALIBRATION OF THE TJNAF HALL-B PHOTON TAGGER AND  
INVESTIGATION OF LIMITATIONS OF THE PHOTON TAGGING TECHNIQUE

---

THESIS

---

A thesis submitted in partial fulfillment of the  
requirements for the degree of Master of Science in the  
Department of Physics and Astronomy  
at the University of Kentucky

By

Marianna Gabrielyan

Lexington, Kentucky

Director: Dr. Daniel Dale, Professor of Physics

Lexington, Kentucky

2006

## TABLE OF CONTENTS

List of Tables .....	iii
List of Figures .....	iv
List of Files .....	vii
Chapter 1: Introduction	
Physics Background and Motivation.....	1
General Description of the Technique.....	2
Chapter 2: Bremsstrahlung Photon Tagger	
Photon Tagging System.....	3
The Dipole Magnet.....	5
The Hodoscope.....	6
The E-plane.....	6
The T-plane.....	7
Chapter 3: Experimental Setup and Technique	
Description of the Experimental Setup.....	9
Flux Normalization with Total Absorption Counter.....	10
The Pair Spectrometer.....	11
Micro Strip Detector.....	13

Chapter 4: Analysis Results

Description of the Data.....16

Results.....18

Chapter 5: Investigation of Limits

    Limitations of the Photon Tagging Technique.....30

    Investigation of Limits.....32

Conclusion and Future Work.....38

Bibliography.....39

Vita.....40



## LIST OF TABLES

Table 4.1 The format of the ntuple.....17

Table 4.2 Relative energies normalized to Eid 350.....25

## LIST OF FIGURES

Fig. 2.1 Layout of the tagging system.....	3
Fig. 2.2 Schematic view of the tagging system.....	5
Fig. 2.3 Section of the hodoscope focal plane showing the orientation of the E- and T- planes with respect to vacuum window and relative positions of E and T counters with a few typical electron trajectories .....	6
Fig. 2.4 Time difference between two electrons detected in the tagger within 20ns time window.....	8
Fig. 3.1 The schematic view of the experimental setup.....	9
Fig. 3.2 Schematic and actual views of Pair Spectrometer.....	11
Fig. 3.3 Schematic view of the pair spectrometer front detector.....	12
Fig. 3.4 Geometry of the planned pair spectrometer.....	13
Fig. 3.5 Photograph of the micro-strip detector.....	14
Fig. 3.6 Distribution of hits on two x- and y- planes.....	14
Fig. 4.1 The x coordinate (in dispersive direction) of the electron is plotted versus that of the positron for fixed Eid and fixed magnetic field.....	18
Fig. 4.2 a) TDC spectrum without cuts (timing between PS and the tagger).....	20

Fig. 4.2 b) Energy distribution of accidental photons, the peak around 3 GeV is because of a hot counter.....	20
Fig. 4.3 Projection histograms in the rotated coordinate system for different PS magnetic fields. The X axis in these plots is $(x_{\text{left}} - x_{\text{right}})/\sqrt{2}$ .....	22
Fig. 4.4 Determination of the magnetic field from a linear fit. The X axis is $(x_{\text{left}} - x_{\text{right}})/\sqrt{2}$ , and the Y axis is B.....	23
Fig. 4.5 Determined magnetic fields vs. Eid (top plot), distances of the determined magnetic fields from a linear fit vs. Eid (bottom plot).....	24
Fig. 4.6 The energy ratios versus Eid, normalized to Eid 350 .....	29
Fig. 5.1 Ratio of cross-sections of electron bremsstrahlung to total bremsstrahlung.....	31
Fig. 5.2 The experimental setup.....	32
Fig. 5.3 Generated photon energy distribution with the scaled position cuts on the leptons.....	34
Fig. 5.4 a) Relative tagging ratios vs T-counter ID for data (blue) and simulation (red).....	35
Fig. 5.4 b) Difference between data and simulation curves.....	35

Fig. 5.5 a),b) Relative tagging ratios vs T-counter ID for different  
PS detectors.....36

Fig. 5.5 c),d) Difference between data and simulation curves.....36

## LIST OF FILES

File 1 MG\_thesis.pdf

# Chapter 1: Introduction

## 1.1 Physics Background and Motivation

The Primakoff experiment [1] is measuring the  $\pi^0$  lifetime with a precision of 1.5%. Experimentally, the  $\pi^0$  photoproduction cross-section is measured and the decay width of the  $\pi^0 \rightarrow \gamma\gamma$  decay is extracted from this cross-section. The determination of the cross-section strongly depends on knowing the photon flux incident on the target. The accurate determination of the incident photon flux in turn depends on knowing the number of photons tagged in each energy bin.

The purpose of this work is to perform the relative energy calibration of the incident photons as measured by the tagging counters of the TJNAF Hall-B photon tagger. Our technique is based on two methods of determining the photon energy, one with the photon tagger and the second, with the pair spectrometer (discussed further in the text).

The calibration of tagging counters is important also for Pentaquark searches. Analysis showed that the photon energies determined by the tagger and reconstructed photon energies from the CLAS (CEBAF Large Acceptance Spectrometer) detector slightly differ. In this case the  $\gamma p \rightarrow p\pi^+\pi^-$  reaction was used to determine photon energies, since it can be fully reconstructed. The kinematic fitting method, which allows the application of energy and momentum conservation laws as physical constraints to improve measurements, was used to determine photon energies from this reaction [2].

## 1.2 General Description of the Technique

In this work the energies of individual photons in a high energy bremsstrahlung beam were determined by two methods. The first method is tagging by the photon tagger, the second method is measuring by the pair spectrometer. We are comparing the photon energies as determined by the photon tagger with those determined by the pair spectrometer [3].

To perform this measurement, micro-strip detectors, designed for high position resolution with  $50\mu\text{m}$  pitch, were mounted near the exit of the pair spectrometer magnet vacuum window to detect electrons and positrons produced in the pair production process, when the photon beam hits the pair converter of the PRIMEX pair spectrometer. In the pair production process the photon produces electron-positron pairs in the Coulomb field of the target nucleus. The target nucleus carries away negligible kinetic energy and thus the sum of the electron and positron energies as determined by the pair spectrometer is assumed to be equal to the incident photon energy. Data have been taken for different magnetic field settings of the pair spectrometer magnet, in order to measure photons with energies from  $0.20E_0$  to  $0.95E_0$ , where  $E_0 = 3.776 \text{ GeV}$  is the initial electron beam energy. For the absolute energy calibration the pair spectrometer alone must be used for bremsstrahlung endpoint measurements, since the corresponding post bremsstrahlung electrons will experience greater curvature and will be out of the acceptance of the photon tagger.

It is necessary for the relative energy calibration to have different pair spectrometer magnetic field settings which will allow us to focus symmetric electron-positron pairs with different energies in the same spot (middle) of the micro strip detectors. By increasing the pair spectrometer magnetic field we will reach the limit when the electron-positron pairs with maximum energy corresponding to bremsstrahlung endpoint will be detected in the micro-strip detectors and after that by increasing the magnetic field no new pairs will be detected, as they will be out of the acceptance of the micro-strip detectors.

## Chapter 2: Bremsstrahlung Photon Tagger

### 2.1 Photon Tagging System

Photon beam production in TJNAF Hall-B is achieved by a photon tagging system or a tagger. The method used to produce photons is the bremsstrahlung radiation process of electrons in the Coulomb field of the nucleus, in which the electrons with initial energy  $E_0$  decelerate in the electromagnetic field of the nucleus. As a result of the negative acceleration, the electrons emit high energy photons. The tagger is designed to tag photons from 20% - 95% of the incident electron energies. It consists of radiators, magnetic spectrometer, collimators and 2 hodoscope planes, called “E” and “T” for energy and timing respectively. Radiators are gold foils ranging from  $10^{-6}$  to  $10^{-4}$  radiation lengths in thickness. A high Z radiator material was chosen to minimize the electron-electron bremsstrahlung process. An overall layout of the tagging system is given in Fig. 2.1 [4].

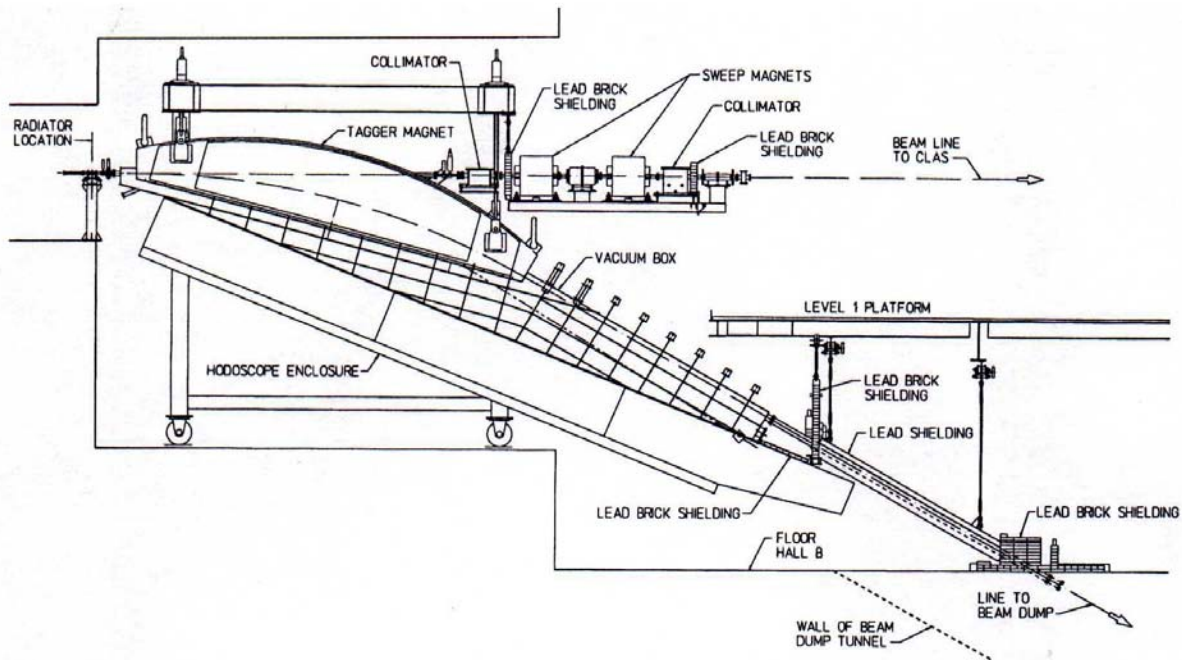


Fig. 2.1 Layout of the tagging system. The approximate length of the tagger magnet is  $\sim 6\text{m}$ . Sweep magnets are necessary to clean up any background that might originate on the walls of collimating system [4].



The electron beam from the accelerator hits the radiator ( $10^{-4}$  r.l.) which is placed in the beam line upstream of the tagger magnet. As a result of the bremsstrahlung radiation some of the electrons lose energy by emitting photons. The characteristic angle of the photon angular distribution is  $\Theta_c = mc^2 / E_0$ . For high energies ( $> 800$  MeV) of the incident electrons, to a good approximation, in the lab frame both electrons and produced photons continue moving in the direction of the incident beam. This mixed beam of electrons and photons then passes through the tagger dipole magnet, which separates electrons from photons. Full energy electrons from the beam, which do not interact in the radiator, are bent into a shielded underground beam dump, while the electrons that lost from 20% to 95% of their initial energy are detected by tagger “E” and “T” counters. Normally, it is assumed that the bremsstrahlung process in which the photons are produced is nuclear coherent, that is the nucleus is left in the ground state ( $e^- + A \rightarrow e^- + \gamma + A$ ). The recoil energy of the nucleus is neglected, so the energy of the photon can be written  $E_\gamma = E_0 - E_e$  according to the energy conservation relation, where  $E_\gamma$  is the energy of the emitted photon,  $E_e$  is the energy of the post-bremsstrahlung electron and  $E_0$  is the initial beam energy.

Other processes can occur in the bremsstrahlung radiator which do not preserve the energy conservation relation  $E_\gamma = E_0 - E_e$ . These include incoherent bremsstrahlung, in which the nucleus is left in an excited state or undergoes nucleon knockout ( $e^- + A \rightarrow e^- + \gamma + X$ ), as well as the electron-electron and double bremsstrahlung. These processes impose potential limitations on the tagging technique at GeV energies. The limitations on the technique will be discussed further in the text.

## 2.2 The Dipole Magnet

The tagger dipole magnet is designed in such a way as to allow operation at electron beam energies up to  $\sim 6.1$  GeV. It is about  $\sim 6$  m long and has an open yoke geometry (Fig. 2.2) [4]. This specific geometry was required to cover photon energies from 0.2 to 0.95 of initial electron energies and also to steer full energy electrons into a shielded beam dump ( $30^\circ$  below the beam line) following a circular arc along the surface of the magnet pole.

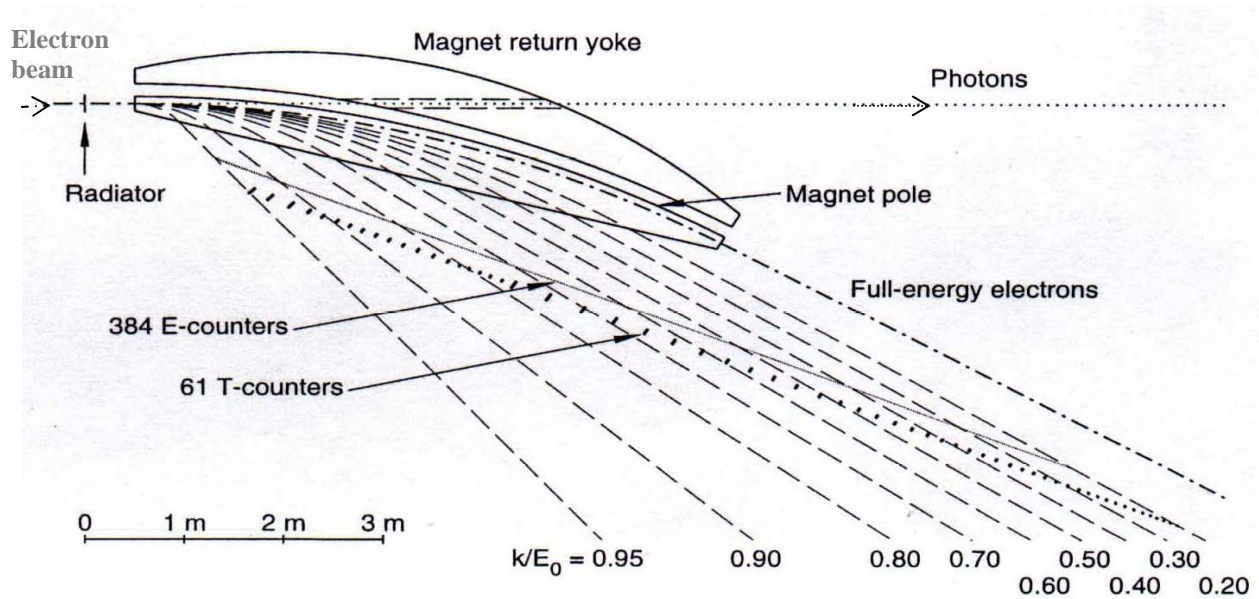


Fig. 2.2 Schematic view of the tagging system. It shows the relative positioning of the “E” and “T” planes. Also some electron trajectories are shown labeled by their recoil energy. [4]

The tests of the uniformity of the magnetic field showed that the energy resolution should be 0.2% or better for electron beam energies below 4 GeV [4]. To minimize the energy loss of post bremsstrahlung electrons due to the multiple scattering, a thin vacuum window is installed, which extends up to the E-plane, leaving the scintillator paddles outside the window to allow easy replacement and repair.

## 2.3 The Hodoscope

The hodoscope focal plane is about 9m long and consists of two rows of scintillator paddles called E- and T- planes for energy and timing respectively. E-paddles must provide the energy of the post bremsstrahlung electrons with sufficient precision to enable  $10^{-3}E_0$  resolution of photon energies. T-paddles must provide timing of the electrons with resolution that will allow associating them with events triggered by corresponding photons. In Fig. 2.3 a section of the hodoscope plane is shown.

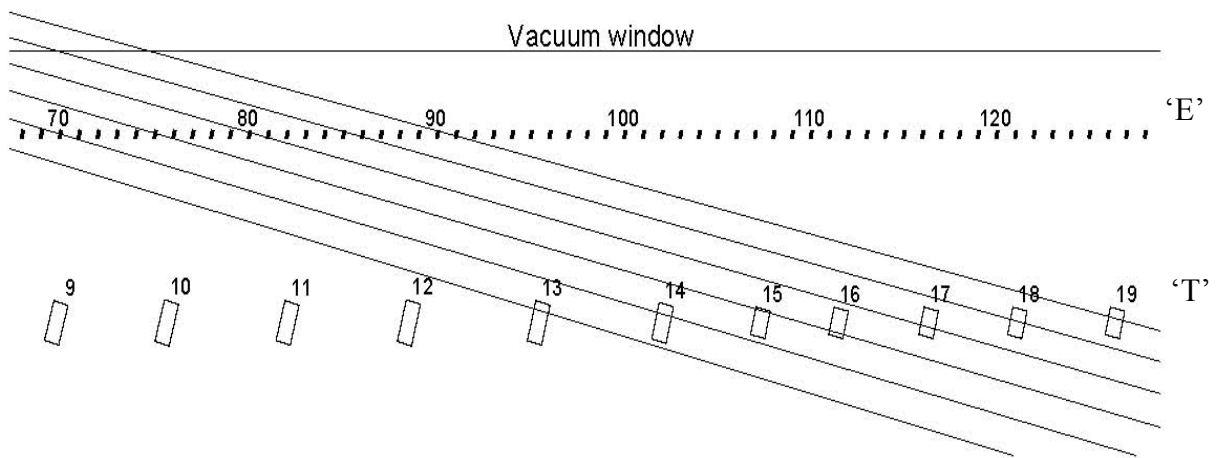


Fig. 2.3 Section of the hodoscope focal plane showing the orientation of the E- and T- planes with respect to vacuum window and relative positions of E and T counters with a few typical electron trajectories [4].

### 2.3.1 The E-plane

The E-plane consists of 384 plastic scintillator paddles (called E-counters) 20cm long and 4mm thick. The widths of the individual scintillators vary from 6 to 18mm to cover almost constant energy intervals of  $0.003E_0$ . The only information necessary to extract from the E-counters are if it was hit or not and the time of the hit. Since the trajectory of the deflected electrons in the magnetic field is a function of momentum, different sections of the focal plane correspond to different particle momenta. Thus, the knowledge of which E counter was hit will provide a

measure of the momentum of the particle. The signals from the E-counter scintillators are transported to the corresponding photomultiplier tubes by optical-fiber light guides. E-counters are mounted in such a way that they overlap by 1/3 of their scintillator area and form 767 fine energy bins by using coincidences and anti-coincidences between neighboring counters, which enables  $0.001E_0$  energy resolution. With the E-counters, common stop multi-hit TDCs have been used (LRS 1877) to record the times of every hit. LRS 1877 multi-hit TDCs have 25ns double pulse resolution, which means that any hit coming within 25ns after the previous one will not be recorded. These multi-hit TDC modules have a programmable LIFO (Last In First Out) limit up to 16 hits per event per channel. If the channel gets more hits than the LIFO limit then the oldest hits are replaced with the newest ones.

The whole focal plane with its corresponding electronics is supported by an Aluminum frame, consisting of four sections each 3.81m long. E-counter scintillators are mounted on aluminum angle rails of three sections. The first two sections are 149.8 inches long and the third one is 85 inches long. The first rail supports E-counters  $E_1$  to  $E_{133}$  (in terms of photon energies  $0.95E_0$ - $0.7E_0$ ), the second supports  $E_{134}$ - $E_{293}$  ( $0.7E_0$ - $0.39E_0$ ) and the third  $E_{294}$ - $E_{384}$  ( $0.39E_0$ - $0.2E_0$ ) [2].

As will be discussed later, the gravitational sagging of these sections of support rails has affected the energy calibration of the tagger. Part of the goal of this work is to quantify this effect.

### **2.3.2 The T-plane**

The T-plane consists of 61 comparatively larger scintillators (T- counters) 2cm thick, with one photomultiplier tube attached to each end of a scintillator. With T-counters the common start single hit TDCs have been used. The single hit TDCs can record only one hit per event per channel, which introduces a slope in the TDC spectrum (Fig 4.2.a).

The T-counters are designed to measure the time of each hit in the tagger with resolution  $\sim 300$ ps or better and used to form a physics trigger between the tagger and the triggering detector. The time difference between two electrons detected in the tagger is shown in Fig. 2.4. Each of the experimental halls receives electron bunches 2ns apart from each other. Beam buckets from the accelerator 2ns apart can be clearly seen from the plot. The widths of the peaks are due to the time resolution of the T-counters.

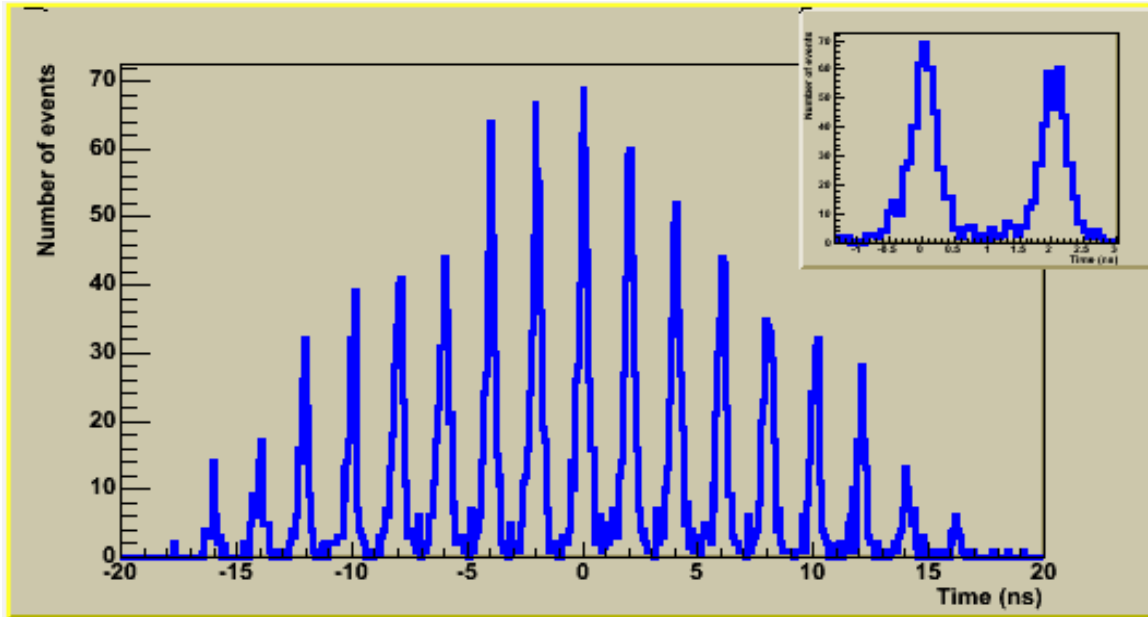


Fig . 2.4 Time difference between two electrons detected in the tagger within 20ns time window. Beam structure with 2ns intervals between beam buckets can be clearly seen from the plot.

Each hit in a tagger is reconstructed by the time coincidences between E-T counters. E-E and T-T time coincidences are applied for overlap regions. Also the TR-TL coincidence cut is applied, which is the time difference between the right and left TDC signals of T-counters.

T-counters are divided into two groups. The top 19 T-counters cover the high energy part of the tagger (from  $0.95E_0$  to  $0.77E_0$  photon energies), the rest of them cover energy ranges from  $0.77E_0$  to  $0.20E_0$ . The lengths of the T-counters vary from 9cm at the low electron momentum end to 20 cm at the high electron momentum end. The sizes of the T-counter scintillators vary in order to provide approximately equal counting rate on each detector within its group. T-counters also have some overlap, the purpose of which is not to allow any gaps between the counters through which the electrons can pass undetected.

## Chapter 3: Experimental Setup and Technique

### 3.1 Description of the Experimental Setup

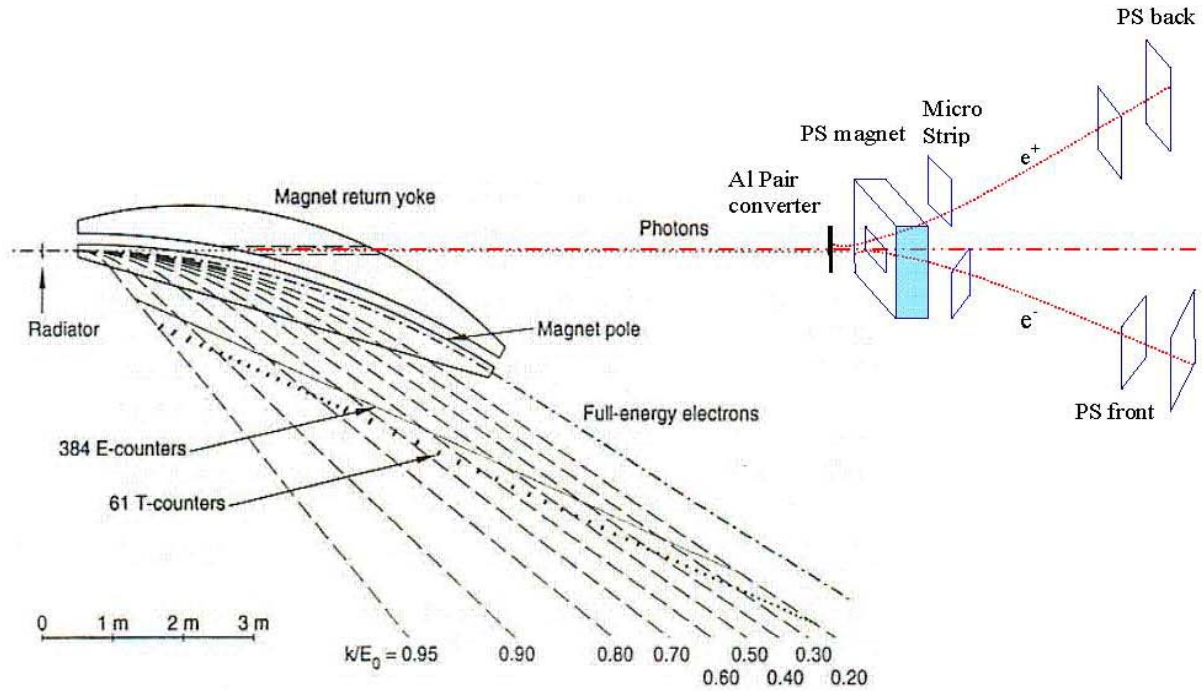


Fig. 3.1 The schematic view of the experimental setup.

A schematic view of the experimental setup is given in Fig. 3.1. The tagged photon beam hits the pair converter ( $10^{-3}$  r.l., Al) located  $\sim 55.8$ cm upstream of the pair spectrometer magnet center. Some of the photons create electron-positron pairs in the electromagnetic field of the nuclei of the converter. Created electron and positron pairs are bent in opposite directions passing through the magnetic field of the pair spectrometer magnet and detected in the micro strip detector assembly and two rows of pair spectrometer detectors. Only two pair spectrometer detectors were 'ON' in the front row and 8 detectors in the back row on each side. The four fold coincidences between pair spectrometer detectors form the trigger. During this measurement data have been taken for pair spectrometer magnetic fields from 0.36T to 1.9T (corresponding currents are 550A to 2775A). The detailed descriptions of the pair spectrometer and the micro strip detector assembly are given in the next sections of the text.

### 3.2 Flux Normalization with Total Absorption Counter

The total absorption counter (TAC) is used as an absolute monitor of the photon flux incident on the target. It consists of a single 20 by 20 by 40 cm<sup>3</sup> lead glass block with one 5 inch PMT attached to it and is also instrumented with both a TDC and ADC. A 100% photon detection efficiency is assumed for the TAC counter.

The absolute calibration of the number of photons is necessary, since the number of photons recorded by tagging counters may not be equal to the number of photons that reach the Primakoff target due to a number of effects:

1. Photons are produced in the bremsstrahlung radiator but are absorbed before reaching to the target.
2. Moller scattering in the bremsstrahlung radiator in which extra electrons will be knocked out from the atoms and reach the tagging counters without producing photons.
3. Extra electrons recorded by the tagging counters due to room background.

For calibration of the first two effects the target is removed from the beam line and the TAC counter is placed in the photon beam. The tagging ratio is determined from the calibration run as the ratio of Tagger • TAC coincidences ( $N_{\gamma}^{\text{tagged}}(\text{calib})$ ) to the tagger events:

$$R^{\text{TAC}} = \frac{N_{\gamma}^{\text{tagged}}(\text{calib})}{N_e(\text{calib})}$$

A thinner radiator is used in calibration runs than in the production runs to reduce the photon flux in order to exclude pile-up. The photon flux in the run can be determined as

$$N_{\gamma}^{\text{tagged}}(\text{experiment}) = N_e(\text{experiment}) \times R^{\text{TAC}}$$

where  $N_e(\text{experiment})$  is the number of electrons in a given tagging counter. The cross section can be extracted from the tagged yield of  $\pi^0$ 's.

$$Y = \frac{d\sigma}{d\Omega} \times t \times \Delta\Omega \times \varepsilon \times N_e(\text{experiment}) \times R^{\text{TAC}}$$

where  $t$  is the target thickness, and  $\Delta\Omega$  is the solid angle of the  $\pi^0$  detector and  $\varepsilon$  is the  $\pi^0$  detection efficiency [5].

The main disadvantage of the TAC counter is that it can operate only at low beam currents. At high beam currents the photon flux is monitored by the pair spectrometer.

### 3.3 The Pair Spectrometer

The Pair Spectrometer (PS) is used as a relative photon flux monitor and designed to operate at higher photon rates (up to  $\sim 10^7$  Hz) than is possible with the Total Absorption Counter (TAC). The pair spectrometer is composed of a dipole magnet and plastic scintillator detectors to detect the electron-positron pairs originating in the target. The schematic and actual views of the pair spectrometer are shown in Fig. 3.2. The photograph is taken from the downstream of the pair spectrometer magnet. The planned pair spectrometer is organized in two rows 32 detectors in each row, 16 on each side (total of 64 detectors) and its geometry is given in Fig. 3.4.

At the time of this measurement only 32 PS detectors were installed 16 front and 16 back. Because of its segmentation the PS can also provide a rough measure of energy. The momentum acceptance of the front detectors is about  $74\text{MeV}/c^2$  for the given geometry of our experimental setup.

The pair spectrometer master true trigger is formed by four-fold coincidences of these detectors (left-right and front-back coincidences).

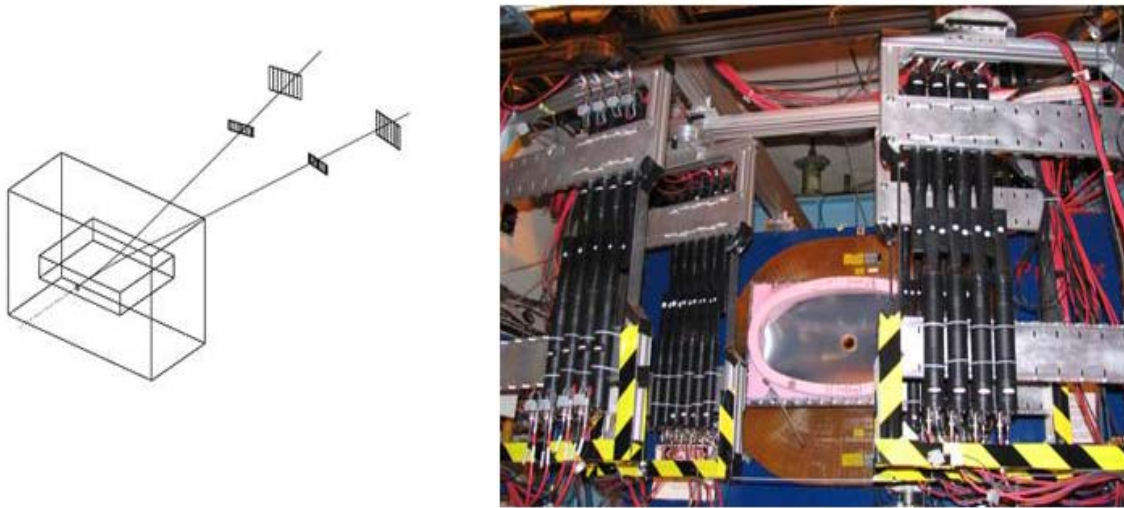


Fig. 3.2 Schematic and actual views of the Pair Spectrometer (PS). In the schematic view the electron beam goes from the lower left to the upper right. The photograph is taken from the downstream of the PS magnet looking upstream. In the photograph the PS magnet and the relative positioning of the two PS detector planes are shown.

The front detectors are comparatively smaller than the back detectors. The distance of the



centers of the front detector planes from the beam line is 25.6cm. They are located 140.1cm from the center of the dipole magnet. The main components of the detectors are the scintillator, light guide and photomultiplier tubes (PMT). The front detector scintillators are 2.4cm wide, 7.5cm long and 5 mm thick. The thicknesses of the scintillators are chosen in such a way that the deflection from the original trajectory of electrons and positrons due to multiple scattering is small. The back detectors are located 186.5cm from the center of the dipole magnet. The distance from the beam line to the centers of the back detectors is 34.0cm. The back detector scintillators are 3.1cm wide, 9.3cm long and 2cm thick. The sizes of the detectors are chosen in such a way that the geometrical acceptance of each front detector corresponds to one back detector  $\pm 1$  (front detector №1 corresponds to back detector №1 $\pm 1$ ). A schematic view of one of the front detectors is given in Fig. 3.3.

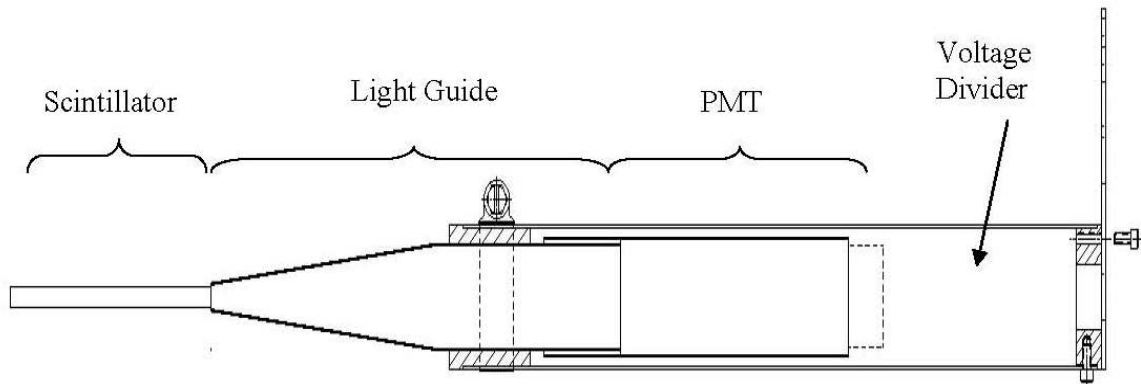


Fig. 3.3 Schematic view of the pair spectrometer front detector.

The central bend angle between the front and back detector plane centers and the beam line is 10.337 degrees.

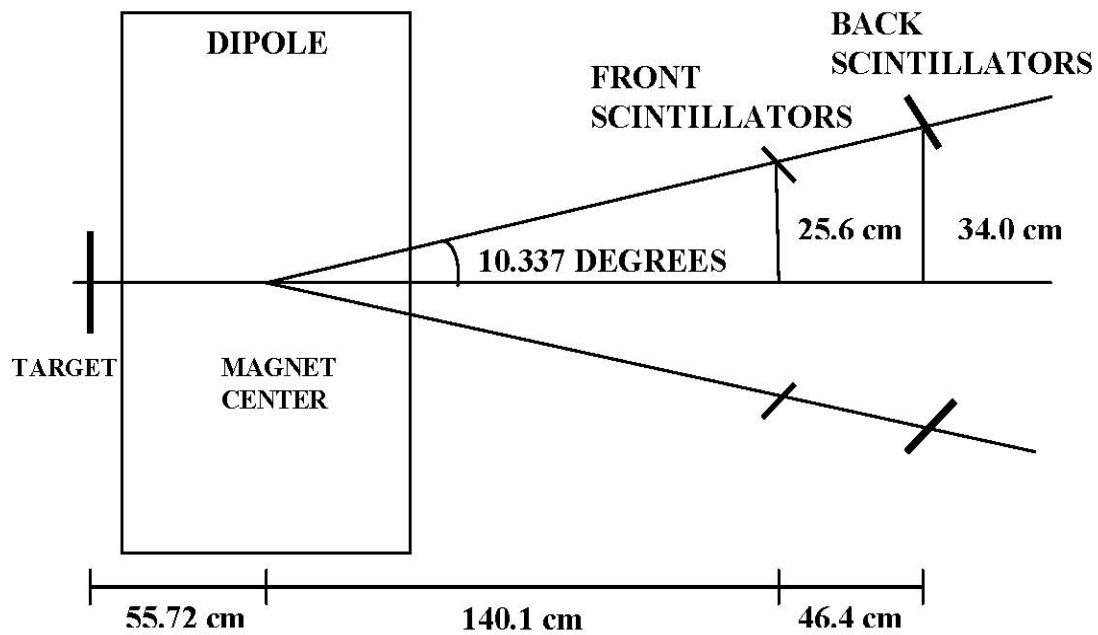


Fig. 3.4. Geometry of the planned pair spectrometer.

### 3.4 Micro Strip Detector

The micro-strip detectors are made of a large number of identical cells, which are also called repetition units, usually in a plane to provide high coordinate resolution in one dimension in that plane. The main geometrical parameter of a micro-strip detector is its pitch (in our case  $50\mu\text{m}$ ), which is the orthogonal distance between the centers of two adjacent repetition units. The spatial resolution of such a detector is determined by the pitch. A picture of one of the micro-strip detectors is shown in Fig. 3.5.

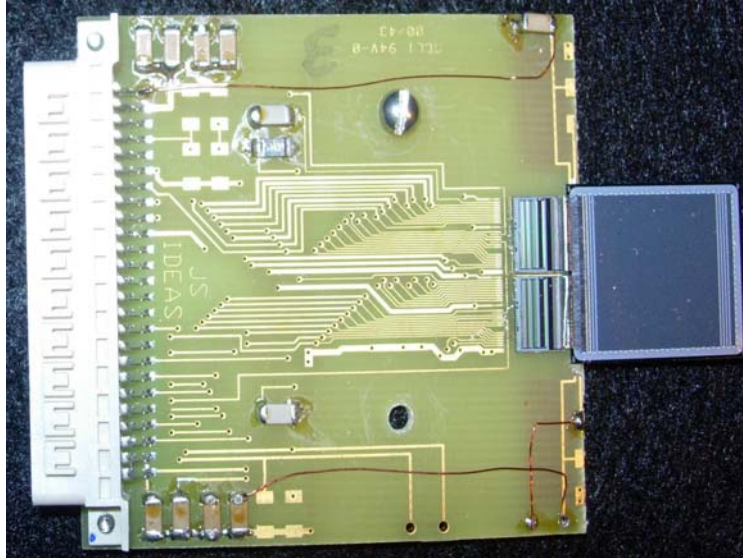


Fig. 3.5 Photograph of the micro-strip detector. The active area of the detector is on the right and the PC board is on the left.

The micro-strip detector assembly consists of two horizontal and two vertical planes. They are located 930.7 mm downstream of the pair spectrometer magnet center. The separation between the centers of two 'X' planes is 450.5mm. Their centers are at the level of the beam line.

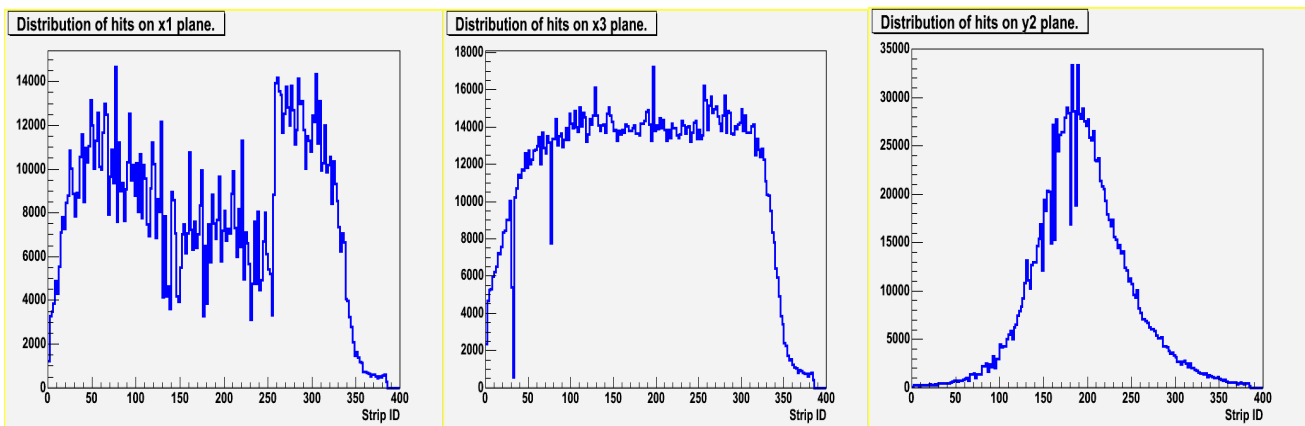


Fig. 3.6 Distribution of hits on two x- and y- planes.

The distributions of the hits on a 'Y' and two 'X' planes are shown in Fig. 3.6. The second vertical plane was not working properly and was not used in the analysis.

The Pair Spectrometer magnetic field sweeps electron-positron pairs only in the horizontal plane. From these plots we can see that the hits are distributed throughout the acceptance of the x-planes and mostly in the middle on y-plane. The sharp drop of the hit distribution histogram of the first x-plane is because of the inefficiency of the strips caused by applied ADC cuts. This will not affect the analysis results except for reducing the statistics, since a coincidence is required between the two 'X' planes.

Despite the fact that the micro-strip detectors have a very good position resolution, multiple scattering in the pair converter can affect the energy resolution. Since the measured energies of the electrons and positrons depend on the bend angle of the electron-positron pairs, as a result of the multiple scattering the bend angle can change, respectively changing the coordinates determined by micro strip detectors.

## **Chapter 4: Analysis Results**

### **4.1 Description of the Data**

The following is the format of the ntuple (Table 4.1). The ntuple is the data structure compatible with PAW, which can store the physical variables and the arrays of the physical variables. Data were recorded on an event by event basis.

Variables are divided into three blocks: EPICS, TAGR and MSD. The information to EPICS block comes from header and epics banks. The TAGR block of the ntuple is filled after the hit reconstruction in the tagger from the tagr bank. The MSD block contains information from micro-strip detectors. The pedestals are subtracted from the ADC values before filling the ntuples.

	<b>BLOCK</b>	<b>Variable</b>	<b>Description</b>
1	EPICS	Run	Run number
2	EPICS	Event	Number of event
3	EPICS	Evntime	Event time with respect to an absolute clock
4	EPICS	x2c21a	x-position on x2c21a Beam Position Monitor (BPM)
5	EPICS	y2c21a	y-position on y2c21a BPM
6	EPICS	c2c21a	Current given by x2c21a BPM
7	EPICS	x2c24a	x-position on x2c24a BPM
8	EPICS	y2c24a	y-position on y2c24a BPM
9	EPICS	c2c24a	Current given by x2c24a BPM
10	EPICS	Pscurrent	Current of PS dipole magnet
11	EPICS	Psprobe	PS dipole Hall probe
12	EPICS	Taggercurrent	Current of tagger dipole magnet
13	EPICS	Taggerprobe	Tagger dipole Hall probe
14	TAGR	Nphot_tagr	Total number of hits in a tagger
15	TAGR	tagr_E_gamma(nphot_tagr)	Photon energy
16	TAGR	tagr_ttag(nphot_tagr)	Photon time measured by tagger
17	TAGR	tagr_tpho(nphot_tagr)	Photon time with a constant correction
18	TAGR	tagr_stat(nphot_tagr)	Reconstruction status (7 or 15 are good)
19	TAGR	tagr_Tid(nphot_tagr)	T-counter ID
20	TAGR	tagr_Eid(nphot_tagr)	E-counter ID
21	MSD	Nmsd	Total number of hits on Micro Strip Detector Assembly (MSD)
22	MSD	msdpl(nmsd)	MSD plane number for each hit
23	MSD	msdid(nmsd)	MSD strip ID for each hit
24	MSD	msdadc(nmsd)	ADC value for each hit

Table 4.1 The format of the ntuple. Shows the three blocks of the variables and arrays.

## 4.2 Results

After the photon beam hits the pair converter, electron-positron pairs are created, which are detected in the micro-strip detectors and the pair spectrometer. The correlation between electron and positron coordinates for fixed energy bin (Eid) and fixed pair spectrometer magnetic field is shown in Fig. 4.1.

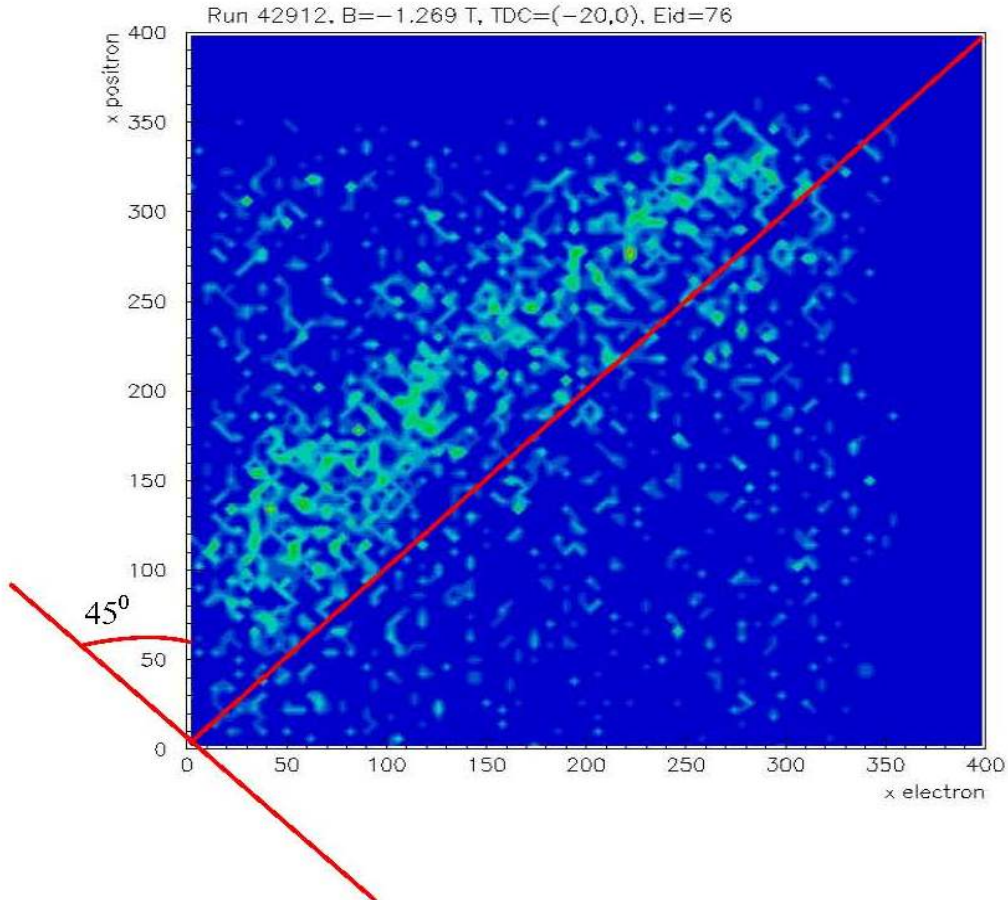


Fig. 4.1 The x coordinate (in dispersive direction) of the electron is plotted versus that of the positron for fixed Eid and fixed magnetic field.

In these plots in order to avoid having negative values on any of the axes, the values on one of the axis is multiplied by (-1), which changes the sign of the slope of the distribution.

For fixed energy channel (Eid) different magnetic field settings move the distribution up or down

along the diagonal within the square. For each Eid we can see the left-right position correlation for several magnetic field settings, or in other words, each magnetic field can cover several energy bins.

A TDC spectrum which is the timing between the PSMT (pair spectrometer master true) signal and the tagger is shown in Fig. 4.2 a). PSMT is the four-fold coincidence between pair spectrometer arms (left and right, front and back). These four-fold coincidences between the pair spectrometer detectors form the trigger.

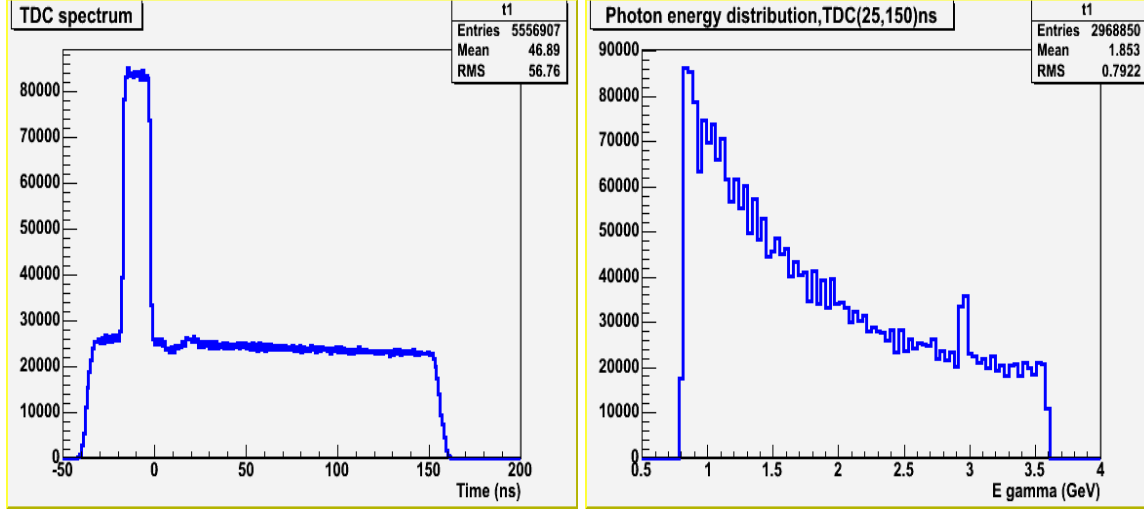
The slope of the distribution in Fig. 4.2 a) is due to single hit TDCs used with the T-counters and the depletion in the region from 0-25ns is due to the dead time effect of the multi-hit TDCs used with E-counters.

In further analysis for the subtraction of accidentals TDC and ADC cuts are applied. In order to avoid double counting hits in a micro strip detector ADC weighted averages of the coordinates

are taken  $\left( \frac{\sum_i strip(i) * adc(i)}{ADC\_Sum} \right)$ . The standard deviation ( $\sigma$ ) from the mean is defined and the

corresponding cut is applied to make sure that the hits on the micro-strip detectors are adjacent and come from the same event. By applying the  $\sigma$  cut we are requiring that each hit be not farther than 6 pitches away from the mean.





a)

b)

Fig. 4.2 a) TDC spectrum without cuts (timing between PS and the tagger). b) Energy distribution of accidental photons, the peak around 3 GeV is because of a hot counter.

Our true events are in the region from -20 to 0 ns. The energy spectrum of accidentals is shown in Fig. 4.2 b) when a TDC cut is applied from 25 to 150 ns. The distribution has the shape of a bremsstrahlung spectrum as expected ( $1/E_\gamma$ ).

For relative energy calibration we need to determine the pair spectrometer magnetic fields required to put electron-positron pairs with different energies in the middle of the micro strip detectors on each side.

Coordinate axes are rotated by 45 degrees in the electron-positron position correlation plot (Fig. 4.1). Then in the rotated coordinate system two dimensional position histograms are projected on the rotated Y axis. An acceptance corrected position projection histogram is created for each magnetic field setting corresponding to each Eid. The acceptance correction is performed for each bin of the one dimensional projection histogram by multiplying its content by a factor determined by its position from 0. In other words this normalization factor is determined as

$$f = \frac{386 \cos(45^\circ)}{386 \cos(45^\circ) - |\text{bin center}|}$$

where number 386 is the maximum number of pitches of the micro-strip detector.

It is normalized to one for the bin centered at 0. The projection histograms for different magnetic field settings are shown in Fig. 4.3.

In order to determine the magnetic fields needed to place the electron-positron pairs in the

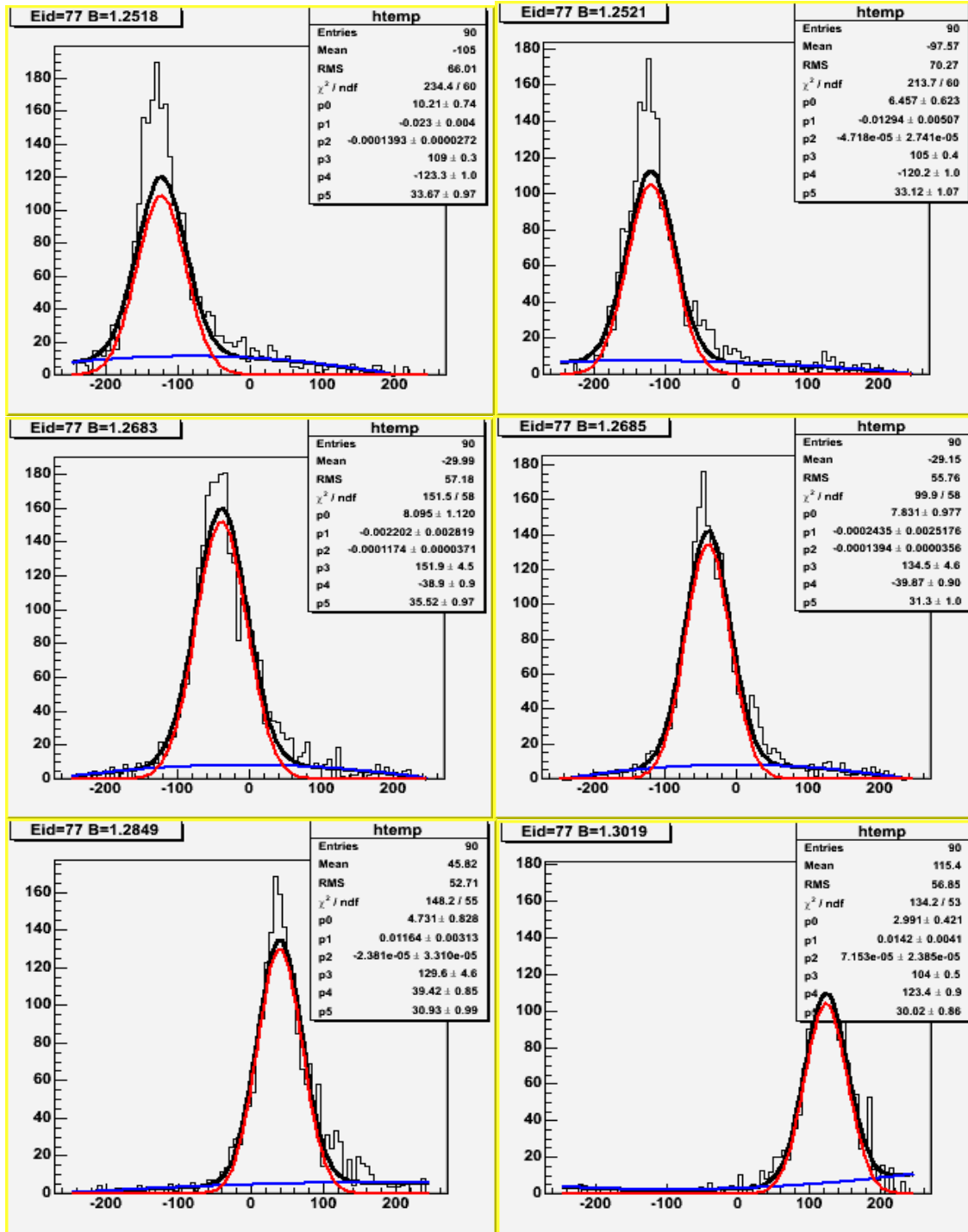


Fig. 4.3 Projection histograms in the rotated coordinate system for different PS magnetic fields. The X axis in these plots is  $(x_{left} - x_{right})/\sqrt{2}$ .

middle of the micro strip detectors, two functions, a Gaussian (red curve) and a second degree polynomial (blue curve) are fitted to the projection histograms (Fig. 4.3). The black curve is the sum of the Gaussian and a second degree polynomial. After finding the peak positions for different magnetic fields and fixed E-bin from the fit function, a line is fitted to these points to determine the magnetic field that places electron-positron pairs in the middle of the micro strip detectors, which corresponds to 0 on the X axis of Fig. 4.4.

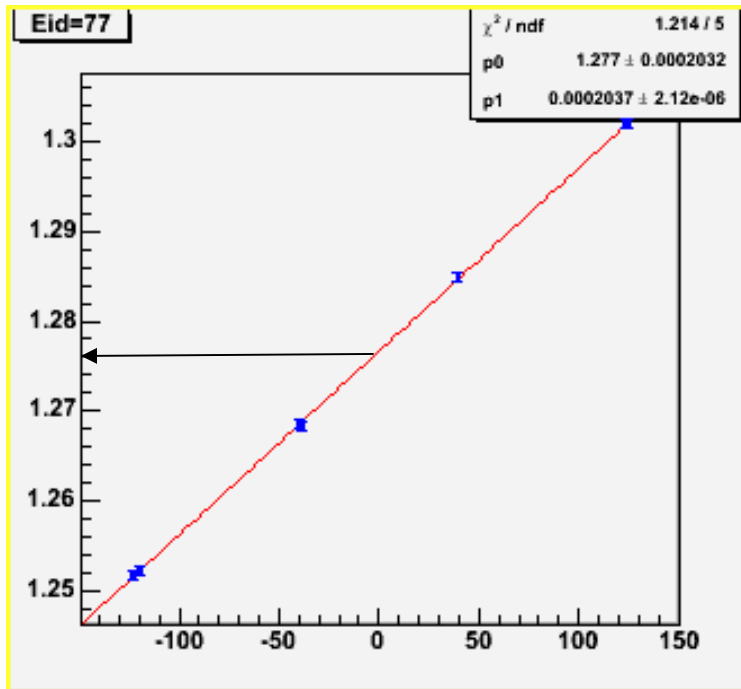
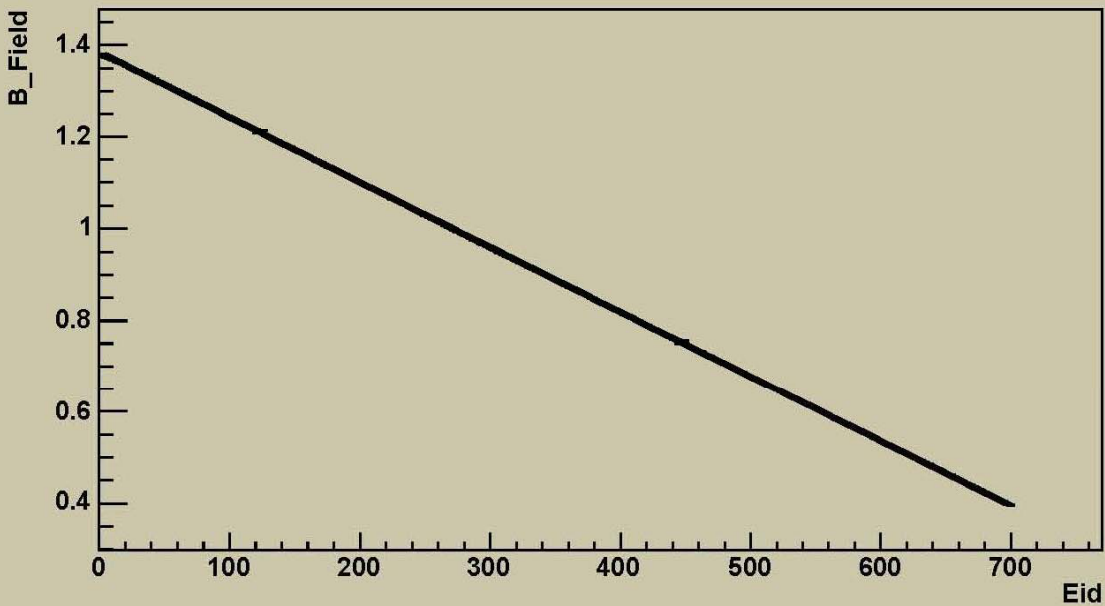


Fig. 4.4 Determination of the magnetic field from a linear fit. The X axis is  $(x_{\text{left}} - x_{\text{right}})/\sqrt{2}$ , and the Y axis is B.

Determined magnetic fields for each tagger Eid as well as deviations of the magnetic fields from a linear fit are calculated and plotted versus Eid. Results are shown in Fig. 4.5. In the bottom plot of Fig. 4.5 the two spikes around Eids 120 and 450 are the result of swapped cables. The small spike around Eid 170 is due to the hot counter. Tagger E counter scintillators are mounted on the aluminum rails supporting the weight of scintillators. These holding rails consist of three sections bolted to each other. The three hump structure that we see around Eid's 270 and 580 of the bottom plot is because of the gravitational deformation of the rails at the positions of the joints. The list of relative energies normalized to E-bin 350 is given in Table 4.1.

### PairSpectrometer Field(T) vs Eid



### Deviation of B from a linear fit

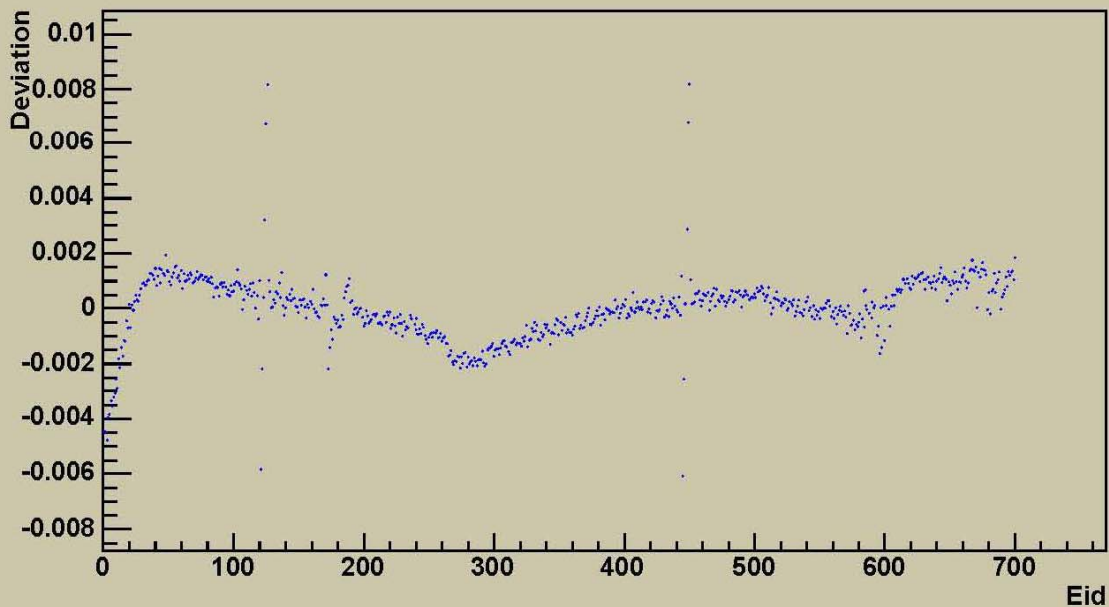


Fig. 4.5 Determined magnetic fields vs. Eid (top plot), distances of the determined magnetic fields from a linear fit vs. Eid (bottom plot).

$E_{id}$	$R = E_{id}/E_{350}$	$E_{id}$	$R = E_{id}/E_{350}$	$E_{id}$	$R = E_{id}/E_{350}$	$E_{id}$	$R = E_{id}/E_{350}$
1	1.55174	176	1.27687	351	0.998906	526	0.720823
2	1.55013	177	1.27618	352	0.996986	527	0.719516
3	1.54819	178	1.27448	353	0.99564	528	0.717829
4	1.54754	179	1.27273	354	0.994019	529	0.71615
5	1.54608	180	1.27125	355	0.992743	530	0.714798
6	1.54504	181	1.2694	356	0.99051	531	0.712575
7	1.54322	182	1.26782	357	0.989041	532	0.71114
8	1.542	183	1.26668	358	0.987354	533	0.709775
9	1.54057	184	1.26493	359	0.98577	534	0.708427
10	1.53956	185	1.2642	360	0.984031	535	0.706316
11	1.53758	186	1.26288	361	0.982715	536	0.704717
12	1.53718	187	1.26151	362	0.981244	537	0.703001
13	1.53524	188	1.25998	363	0.980117	538	0.701667
14	1.53448	189	1.25863	364	0.978454	539	0.700381
15	1.53252	190	1.25607	365	0.976988	540	0.698832
16	1.53158	191	1.25456	366	0.974779	541	0.697424
17	1.52995	192	1.25239	367	0.973314	542	0.695261
18	1.52918	193	1.25104	368	0.971613	543	0.693805
19	1.5273	194	1.2495	369	0.970056	544	0.691849
20	1.52666	195	1.24763	370	0.968716	545	0.690698
21	1.52413	196	1.24612	371	0.967297	546	0.688559
22	1.52346	197	1.24467	372	0.965856	547	0.687339
23	1.52165	198	1.2431	373	0.964449	548	0.68551
24	1.52044	199	1.24115	374	0.962209	549	0.684096
25	1.51909	200	1.2392	375	0.96059	550	0.682212
26	1.5173	201	1.2377	376	0.959089	551	0.681021
27	1.51565	202	1.23663	377	0.957642	552	0.679397
28	1.51432	203	1.23482	378	0.956191	553	0.677839
29	1.51297	204	1.23292	379	0.954804	554	0.676243
30	1.5116	205	1.2314	380	0.953003	555	0.674871
31	1.51004	206	1.2299	381	0.95177	556	0.673389
32	1.50834	207	1.22851	382	0.94942	557	0.671793
33	1.50676	208	1.22691	383	0.948274	558	0.669963
34	1.50534	209	1.22528	384	0.946697	559	0.667964
35	1.5038	210	1.22377	385	0.94487	560	0.666568
36	1.50246	211	1.22178	386	0.943753	561	0.664687
37	1.50086	212	1.22018	387	0.942106	562	0.663536
38	1.49919	213	1.21864	388	0.940482	563	0.661277
39	1.49744	214	1.21696	389	0.938752	564	0.660076
40	1.49628	215	1.2157	390	0.937238	565	0.658654
41	1.494	216	1.21413	391	0.935632	566	0.657234
42	1.49279	217	1.21229	392	0.934008	567	0.65542
43	1.49152	218	1.21109	393	0.932939	568	0.65368

44	1.48933	219	1.20936	394	0.930993	569	0.65226
45	1.48828	220	1.20791	395	0.92949	570	0.650409
46	1.48653	221	1.20565	396	0.927447	571	0.648157
47	1.48486	222	1.20421	397	0.926038	572	0.647695
48	1.48409	223	1.20291	398	0.924656	573	0.645802
49	1.48187	224	1.20099	399	0.923199	574	0.643714
50	1.48024	225	1.19911	400	0.921526	575	0.642152
51	1.47823	226	1.19815	401	0.920231	576	0.640745
52	1.47651	227	1.19631	402	0.917881	577	0.638766
53	1.47526	228	1.19508	403	0.916446	578	0.637407
54	1.47383	229	1.19311	404	0.914785	579	0.635705
55	1.47245	230	1.191	405	0.913518	580	0.634288
56	1.47092	231	1.19001	406	0.911834	581	0.633028
57	1.46883	232	1.18809	407	0.910947	582	0.630464
58	1.46736	233	1.18663	408	0.908572	583	0.629633
59	1.46552	234	1.18498	409	0.90714	584	0.627716
60	1.46436	235	1.18498	410	0.905799	585	0.627627
61	1.46203	236	1.18231	411	0.904009	586	0.625261
62	1.46105	237	1.18056	412	0.902294	587	0.625038
63	1.45915	238	1.17933	413	0.900814	588	0.621901
64	1.45762	239	1.17746	414	0.899119	589	0.62088
65	1.4562	240	1.17535	415	0.897823	590	0.618555
66	1.45448	241	1.17358	416	0.896267	591	0.617533
67	1.45312	242	1.17198	417	0.894732	592	0.615849
68	1.45145	243	1.17059	418	0.892651	593	0.614124
69	1.44952	244	1.16883	419	0.891189	594	0.611447
70	1.44802	245	1.16763	420	0.889404	595	0.610245
71	1.44656	246	1.16588	421	0.88823	596	0.607524
72	1.44521	247	1.16397	422	0.886726	597	0.607811
73	1.4433	248	1.16222	423	0.885084	598	0.6046
74	1.44179	249	1.16045	424	0.882848	599	0.604666
75	1.4403	250	1.15912	425	0.88155	600	0.601836
76	1.43868	251	1.15764	426	0.87993	601	0.601865
77	1.43691	252	1.15611	427	0.878417	602	0.599882
78	1.43544	253	1.15432	428	0.877038	603	0.598208
79	1.43387	254	1.15296	429	0.875758	604	0.595917
80	1.43208	255	1.15134	430	0.874005	605	0.595117
81	1.43061	256	1.14983	431	0.871742	606	0.593993
82	1.42886	257	1.14794	432	0.870217	607	0.591968
83	1.42747	258	1.14638	433	0.868845	608	0.590808
84	1.42561	259	1.14495	434	0.866995	609	0.590518
85	1.42348	260	1.14303	435	0.866005	610	0.587772
86	1.42226	261	1.14157	436	0.864324	611	0.586268
87	1.4207	262	1.14003	437	0.862544	612	0.58455
88	1.4191	263	1.13815	438	0.861356	613	0.583063

89	1.41715	264	1.13655	439	0.859441	614	0.5819
90	1.41604	265	1.13445	440	0.857711	615	0.580306
91	1.4145	266	1.13293	441	0.856019	616	0.578549
92	1.41276	267	1.13151	442	0.855051	617	0.57714
93	1.41135	268	1.12945	443	0.852707	618	0.575356
94	1.40957	269	1.12775	444	0.852707	619	0.57358
95	1.40767	270	1.12631	445	0.842963	620	0.571924
96	1.40625	271	1.12471	446	0.845337	621	0.570876
97	1.40443	272	1.12331	447	0.846799	622	0.568956
98	1.40326	273	1.12169	448	0.848256	623	0.56762
99	1.40141	274	1.11964	449	0.851058	624	0.566005
100	1.39982	275	1.1185	450	0.851058	625	0.564496
101	1.39852	276	1.11667	451	0.841426	626	0.562976
102	1.39704	277	1.11547	452	0.838845	627	0.561107
103	1.39594	278	1.11391	453	0.837285	628	0.559837
104	1.3938	279	1.11174	454	0.835726	629	0.558291
105	1.3921	280	1.11054	455	0.834474	630	0.556395
106	1.39038	281	1.10868	456	0.832909	631	0.554429
107	1.38793	282	1.10715	457	0.831396	632	0.553237
108	1.38676	283	1.10561	458	0.829452	633	0.551741
109	1.38571	284	1.10381	459	0.827587	634	0.549934
110	1.38393	285	1.10252	460	0.82624	635	0.54828
111	1.38219	286	1.1008	461	0.824921	636	0.546502
112	1.38079	287	1.09905	462	0.823289	637	0.545176
113	1.37945	288	1.09768	463	0.821657	638	0.543816
114	1.37734	289	1.09611	464	0.8202	639	0.541695
115	1.37629	290	1.0945	465	0.817878	640	0.540415
116	1.3743	291	1.09328	466	0.816655	641	0.538937
117	1.37207	292	1.09122	467	0.815269	642	0.53754
118	1.37099	293	1.08947	468	0.81379	643	0.536202
119	1.36843	294	1.08797	469	0.812431	644	0.534019
120	1.36843	295	1.08695	470	0.810088	645	0.53258
121	1.35914	296	1.08544	471	0.809184	646	0.531054
122	1.36162	297	1.08385	472	0.807163	647	0.529354
123	1.36296	298	1.08231	473	0.805515	648	0.52689
124	1.36453	299	1.08084	474	0.804144	649	0.526078
125	1.36691	300	1.07872	475	0.802464	650	0.524331
126	1.36691	301	1.07738	476	0.800932	651	0.522399
127	1.35727	302	1.07584	477	0.799133	652	0.521354
128	1.35522	303	1.07425	478	0.797347	653	0.519634
129	1.35298	304	1.07244	479	0.795892	654	0.518525
130	1.35143	305	1.07109	480	0.794448	655	0.516518
131	1.35011	306	1.0697	481	0.792984	656	0.514613
132	1.34839	307	1.06821	482	0.791618	657	0.513339
133	1.34727	308	1.06663	483	0.790005	658	0.511708



134	1.3456	309	1.06482	484	0.787972	659	0.510336
135	1.34444	310	1.0632	485	0.786453	660	0.508843
136	1.34225	311	1.06138	486	0.785193	661	0.507518
137	1.3417	312	1.05971	487	0.783568	662	0.505403
138	1.33873	313	1.05861	488	0.782069	663	0.503512
139	1.33676	314	1.057	489	0.78028	664	0.502128
140	1.33547	315	1.05547	490	0.778213	665	0.50106
141	1.3343	316	1.05395	491	0.77703	666	0.49951
142	1.3326	317	1.05212	492	0.77549	667	0.498291
143	1.33125	318	1.05061	493	0.774075	668	0.496308
144	1.32938	319	1.04898	494	0.772342	669	0.494673
145	1.32826	320	1.0474	495	0.770728	670	0.493228
146	1.32628	321	1.04571	496	0.768954	671	0.489978
147	1.32472	322	1.04444	497	0.767424	672	0.489828
148	1.32279	323	1.04273	498	0.765875	673	0.488073
149	1.32116	324	1.04132	499	0.764241	674	0.486789
150	1.31934	325	1.04018	500	0.762837	675	0.485455
151	1.31826	326	1.03771	501	0.761071	676	0.483567
152	1.31648	327	1.03637	502	0.759881	677	0.481947
153	1.31508	328	1.03485	503	0.758119	678	0.480178
154	1.31355	329	1.03369	504	0.756595	679	0.477169
155	1.3116	330	1.03196	505	0.755186	680	0.476281
156	1.30958	331	1.03075	506	0.753494	681	0.473811
157	1.30853	332	1.0288	507	0.751674	682	0.473143
158	1.3068	333	1.02744	508	0.749812	683	0.471621
159	1.30548	334	1.02528	509	0.748369	684	0.470688
160	1.30376	335	1.02365	510	0.746854	685	0.468304
161	1.30278	336	1.02239	511	0.745575	686	0.467099
162	1.30038	337	1.02062	512	0.743369	687	0.465634
163	1.29865	338	1.0191	513	0.7413	688	0.464377
164	1.29709	339	1.01793	514	0.739973	689	0.46127
165	1.29534	340	1.01619	515	0.738768	690	0.46016
166	1.29365	341	1.01474	516	0.737138	691	0.458709
167	1.29257	342	1.0129	517	0.735847	692	0.457262
168	1.29096	343	1.01075	518	0.733922	693	0.456214
169	1.28966	344	1.00962	519	0.73229	694	0.454236
170	1.28781	345	1.00804	520	0.730503	695	0.453245
171	1.28745	346	1.0064	521	0.729021	696	0.4515
172	1.28463	347	1.00517	522	0.727417	697	0.45002
173	1.28042	348	1.00381	523	0.725992	698	0.448489
174	1.27972	349	1.00217	524	0.724343	699	0.446547
175	1.27883	350	1	525	0.722346	700	0.445843

Table 4.2 Relative energies normalized to Eid 350.

## Chapter 5: Investigation of Limits

### 5.1 Limitations of the Photon Tagging Technique

The conventional photon tagging technique is based on the bremsstrahlung radiation process of electrons in the Coulomb field of a nucleus and implicitly assumes that all photons are produced in a coherent process, so that the nuclei do not undergo a nucleon knockout and are left in the ground state.

The energy of the produced photon is determined as a difference between the initial and final electron energies (the small recoil of the nucleus is neglected).

As the energy of the incident electrons increases and becomes compatible with nuclear excitation energies, then in principle the nuclei can be left in some excited state or undergo nucleon knockout. This is what we call here incoherent bremsstrahlung [6]. Gil and Oset have performed model dependent calculations of quasielastic knockout and its effect on the validity of the tagging technique at high energies [6]. While the specific kinematics of their calculation does not permit a direct comparison with our experimental conditions, the authors do point out that these effects could be important in the several GeV range.

A few other effects may occur in the bremsstrahlung radiator, such as radiative Moller scattering in which case the electrons are scattered off the atomic electrons and double bremsstrahlung where two photons are produced instead of one. When these effects occur, the tagger indicates photon energy higher than it really is.

Relative energies are determined by the relation  $E_i / E_j = B_i / B_j$  which holds in the case of the uniform magnetic fields. The energy ratios vs. Eid normalized to Eid 350 is given in Fig.4.6.

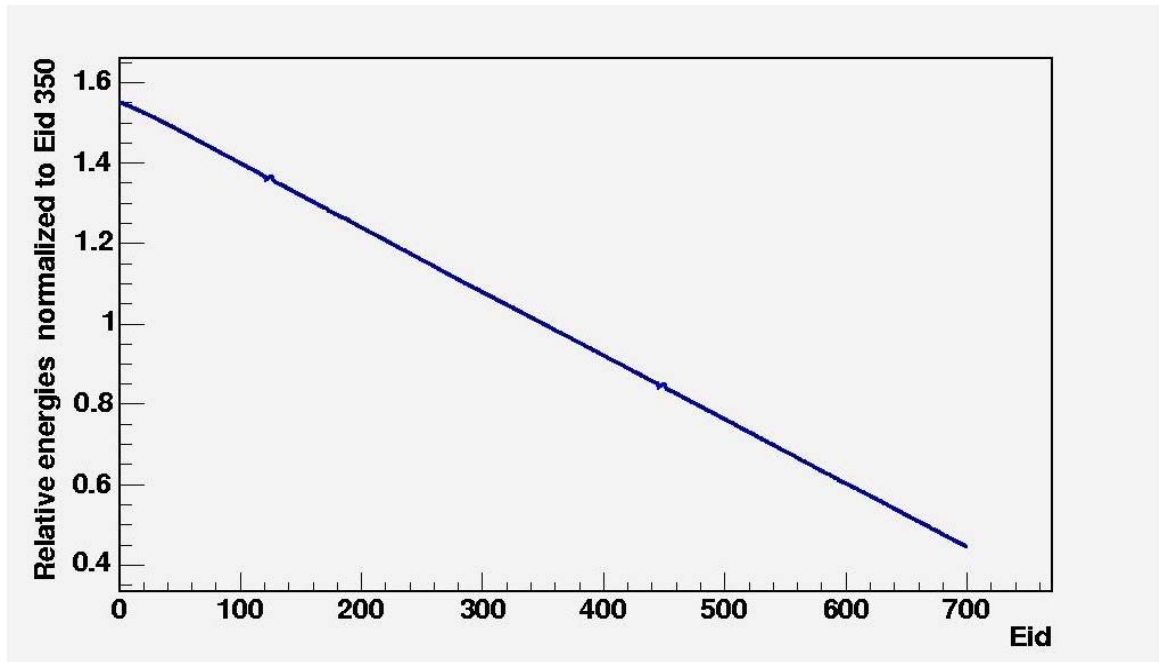


Fig. 4.6 The energy ratios versus Eid normalized to Eid 350.

The gravitational deformation effects disappear when the relative energies are calculated (Fig. 4.6). Again, the spikes around E-ids 120 and 450 are the result of swapped cables. This completes the relative energy calculations.

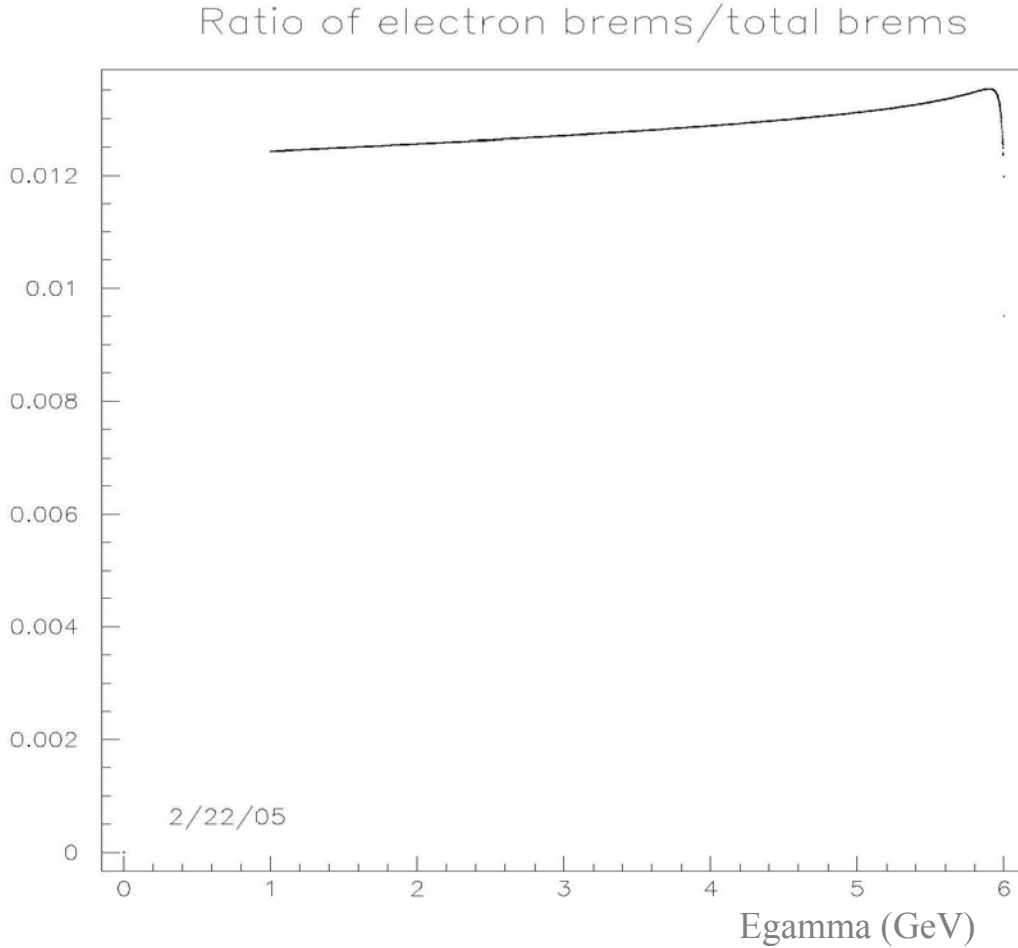


Fig.5.1 Ratio of cross-sections of electron bremsstrahlung to total bremsstrahlung.

These effects may affect both the flux determination and the energy calibration. Until now the precise calibration of Hall-B photon tagger was not performed, because none of the previously proposed experiments needed 0.1% precision in photon energy. PRIMEX is a high precision experiment, measuring  $\pi^0$  lifetime with an accuracy of 1.5%. The lifetime is proportional to  $\pi^0$  decay cross-section, and the cross-section is proportional to photon flux. The normalization of the cross-section of  $\pi^0$  decay process to the incident photon flux depends on knowing the number of tagged photons in each energy bin.

The total bremsstrahlung cross-section depends on  $Z$  as

$$\sigma(Z, T, k_c) = \frac{Z(Z + \xi_\sigma)(T + m)^2}{T(T + 2m)} [\ln(T/k_c)]^\alpha F_\sigma(Z, X, Y) \quad (\text{barn})$$

where  $m$  is the mass of the electron,  $T$  is its kinetic energy,  $Z$  is the atomic charge,  $k_c$  is the

photon energy cut-off,  $X=\ln(E/m)$ ,  $Y=\ln(v_\sigma E/k_c)$  for the total cross-section  $\sigma$ , with  $E = T + m$ . The  $\xi_\sigma$ ,  $\alpha$ ,  $v_\sigma$  are constant parameters [7]. The nuclear bremsstrahlung cross-section is  $Z^2$  dependent, while the atomic bremsstrahlung cross-section is  $Z$  dependent.

Theoretical calculations show that the radiative Moller scattering is  $\sim 1.2\%$  effect (Fig. 5.1) for  $Z=79$  (gold radiator).

The model dependent theoretical calculations of incoherent bremsstrahlung [6] and double bremsstrahlung [8], [9] need to be averaged over the acceptance of the tagger and the experimental setup. So, instead of calculating we decided to measure these effects.

## 5.2 Investigation of Limits

The photon energy can be determined both by the tagger and by the pair spectrometer. The idea again is to compare photon energy  $E_\gamma$  as determined by the tagger with  $E_\gamma$ , as determined by the pair spectrometer. For the investigation of limits the data set from the Fall 2004 PrimEx run have been used. The experimental setup is shown in Fig. 5.2. The electron beam energy in this case is 5.75 GeV.

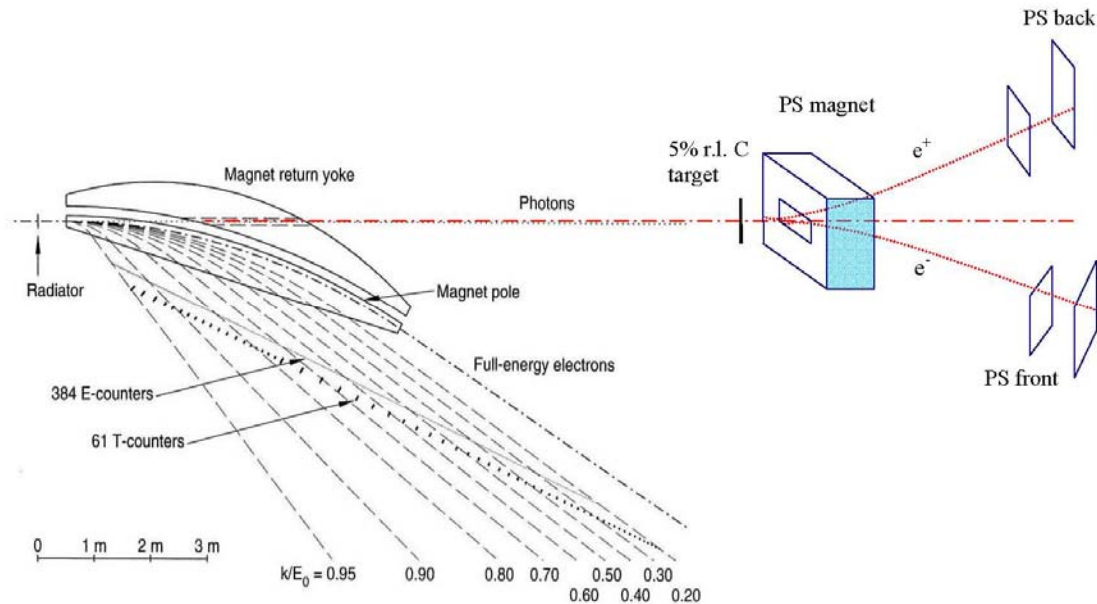


Fig. 5.2 The experimental setup. The electron beam energy is 5.75 GeV. The pair converter is a 5% r.l. C.

Determination of photon energy with high resolution is also complicated by the effects that occur in the pair spectrometer target, such as pair production followed by bremsstrahlung and multiple scattering, in which case the correlation between the energy of the photon and the bend angles of the leptons is weakened. For the investigation of the limits we are comparing experimental results with the GEANT simulation of the setup. The same conditions are used for the simulation as for the experiment. Photons are generated with a  $\frac{1}{E_\gamma}$  bremsstrahlung spectrum

and allowed to hit the 5% r. l. C target. Simulated electron-positron pairs are allowed to pass through the magnetic field of the pair spectrometer dipole magnet ( $I_{ps}= 3105.43A$ ) and registered in a volume, simulating the pair spectrometer detector plane, placed 232 cm from the target. The simulation gives the perfect tagger case (i.e. no incoherent bremsstrahlung, radiative Moller or double bremsstrahlung) with the pair spectrometer effects present. In the actual experiment both tagger and the pair spectrometer effects are present, so any difference between data and simulation can be attributed to tagger effects. The pair spectrometer effects are subtracted off.

The simulations were carried out both for 1% r. l. and 5% r. l. C targets. If there were no pair spectrometer effects, then there should have been a one to one correspondence between the photon energies as determined by the tagger and those determined by the pair spectrometer. This corresponds to the peak in Fig. 5.3.

The spatial cuts on the simulated data took into account the tilt and the actual z-position of the rear pair spectrometer detectors. By applying the position cuts on the leptons the momentum acceptance is fixed. Fig. 5.3 shows the spectrum of the generated photons for the position cuts on both sides of the beam line which correspond to the size of the rear pair spectrometer detectors. Tails on either side of the peak correspond to pair spectrometer effects. For instance when a photon undergoes pair production followed by bremsstrahlung, the result of this will show up on the right side of the peak in Fig. 5.3. This is the region where the  $E_\gamma$  determined by the tagger is higher than that determined by the pair spectrometer.

As expected, the histograms show that making the target thinner is equivalent to reducing these effects. In the limit of an infinitely thin target the pair spectrometer effects will be turned off, since the two-step processes are proportional to  $t^2$  and one-step processes are proportional to  $t$ , where  $t$  is the target thickness.

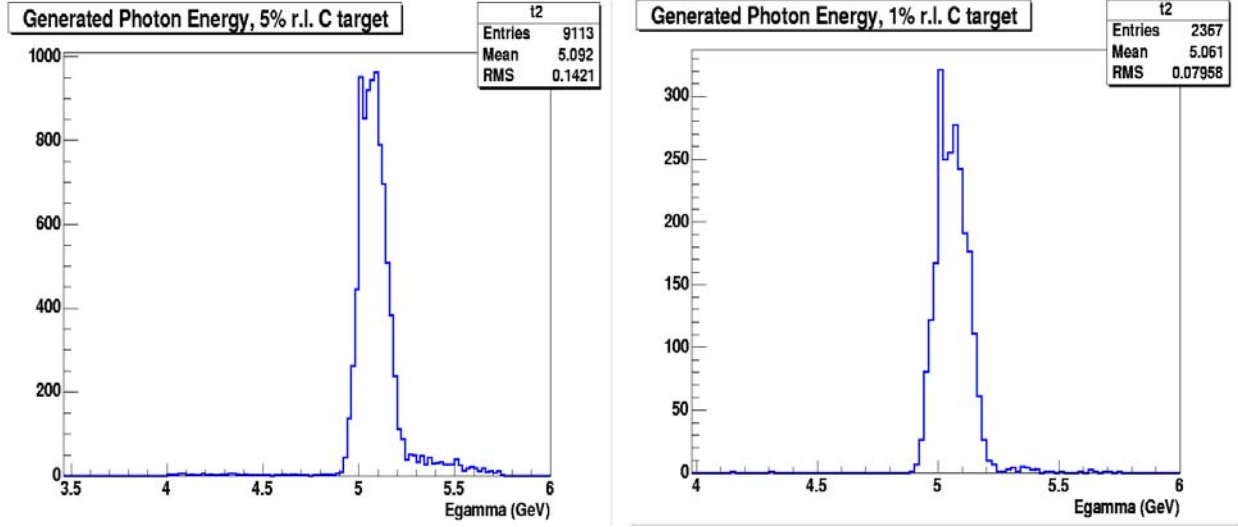


Fig. 5.3 Generated photon energy distribution with the scaled position cuts on the leptons.

In the analysis, the relative tagging ratios normalized to number of photons are compared. The relative tagging ratio in the analysis of the experimental data is determined as the number of pair production events which are in coincidence with an  $e^-$  in a particular T-counter divided by the number of photons associated with the same T-counter:  $R_{\text{experiment}} = \frac{N_{e+e^-} \cdot T_i}{N_{\gamma_i}}$

where  $N_{\gamma_i} = N_{e_i} R_i^{\text{TAC}}$ .  $R_i^{\text{TAC}} = \frac{T_i \cdot \text{TAC}}{T_i^{\text{total}}}$  is the tagging ratio determined with total absorption counter (TAC).

The relative tagging ratio in the analysis of the simulation data is determined as the number of pair production events which are in coincidence with a photon within the energy range covered by a particular T-counter divided by the number of simulated photons within the same energy

$$\text{range: } R_{\text{simulation}} = \frac{N_{e+e^-} \cdot \gamma(\Delta E)_i}{N_{\gamma(\Delta E)_i}}$$

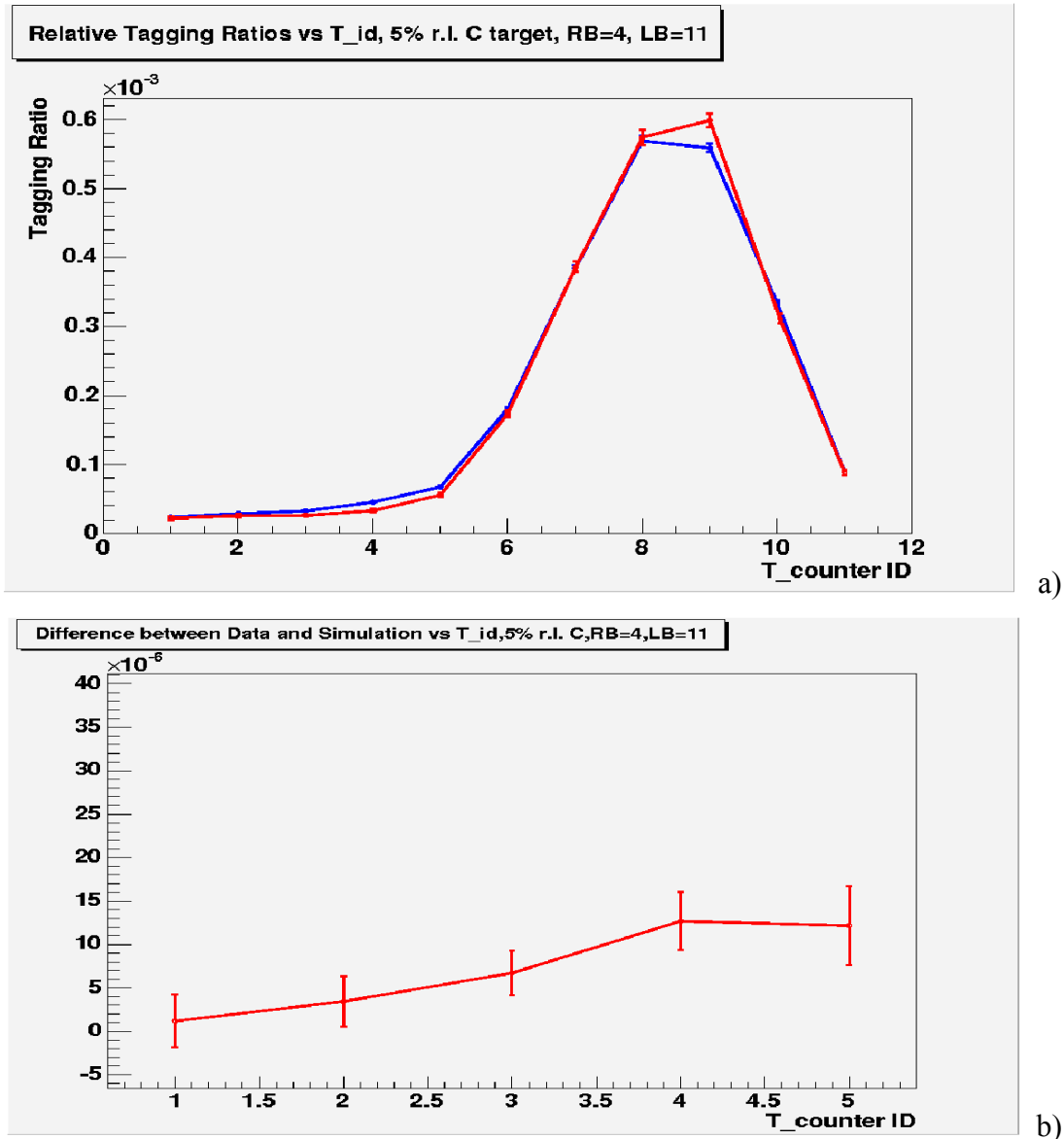


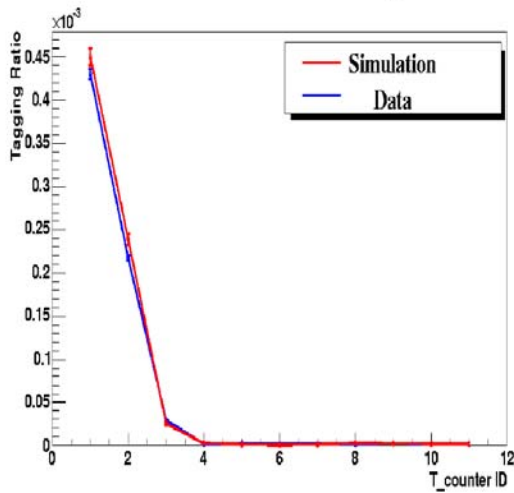
Fig. 5.4 a) Relative tagging ratios vs T-counter ID for data (blue) and simulation (red), b) difference between data and simulation curves.

Fig. 5.4 a) shows the comparison of data (blue) and simulation (red) curves, and b) shows the difference between those curves.

The data curve lies higher than the simulation in the high photon energy tail (high  $E_\gamma$  corresponds to lower T-counter ID) of Fig. 5.4. These are the events that were supposed to be registered in the peak region but due to the tagger and pair spectrometer effects are shifted towards the tail. The compensating depletion appears in the peak region.

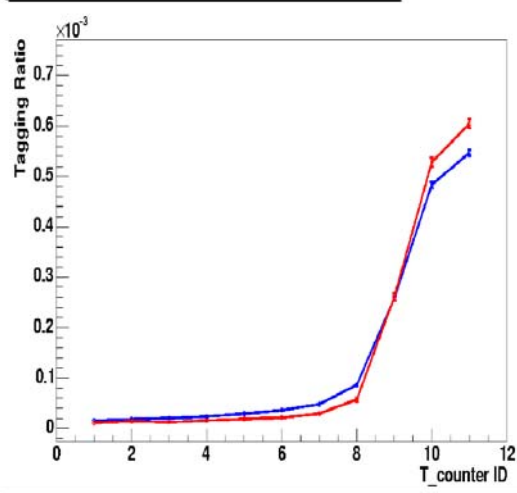


Relative Tagging Ratios vs T\_id, 5% r.l. C target, RB=7, LB=11



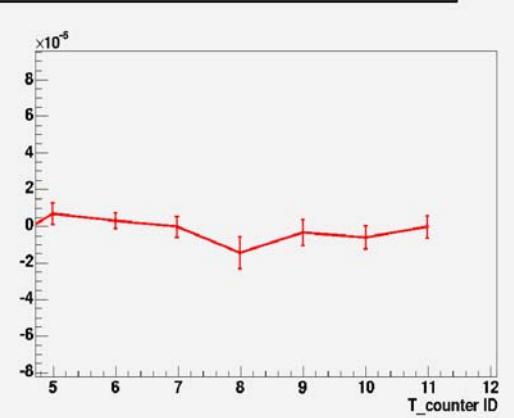
a)

Relative Tagging Ratios vs T\_id,5% r.l. C target, RB=3, LB=11



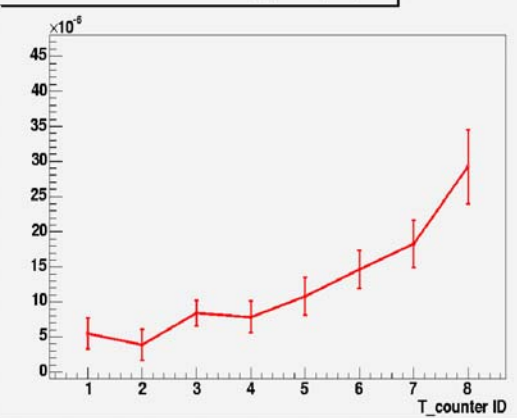
b)

Difference between Data and Simulation vs T\_id,5% r.l. C, RB=7, LB=11



c)

Difference between Data and Simulation vs T\_id,5% r.l. C, RB=3, LB=11



d)

Fig. 5.5 a),b) Relative tagging ratios vs T-counter ID for different PS detectors, c),d) difference between data and simulation curves.

By fixing different pair spectrometer detector positions (i.e. changing momentum acceptance) the peak can be moved towards the higher or lower photon energy regions (again higher photon energies correspond to lower T-counter ID).

In the low photon energy region, the difference between the data and simulation curves is expected to be zero within the error bars, since the effects previously discussed (incoherent bremsstrahlung, double bremsstrahlung, radiative Moller scattering) affect only the high photon energy region. This is what we are seeing from Fig. 5.5 a) and c). This would not be the case if

the accidentals were not properly subtracted. By moving the peak all the way towards the lower photon energies (i.e. varying the lepton position cuts), we can increase the region where the tagger and pair spectrometer effects are observable Fig. 5.5 b). By taking the difference between the data and simulation curves Fig. 5.5 d), we see that the tagger effects are persistent within the error bars, when the photon energy is measured with 0.1%  $E_0$  resolution. As such, we definitely see the signature for these effects which will limit the validity of the photon tagging technique [10]. We emphasize that this result is of general interest for all high precision experiments utilizing the bremsstrahlung photon tagging technique.

## Conclusion and Future Work

In summary, we report on two sets of measurements involving the JLab Hall-B photon tagger and the PrimEx pair spectrometer.

The first measurement employed a series of high position resolution micro-strip detectors to perform a relative energy calibration of the tagging counters. Deviations of our results with the previous calibration are consistent with geometrical deformation of the E counter support rails due to gravitational sagging.

The second set of measurements, collected in conjunction with the Fall 2004 PrimEx run, investigated inherent limitations on the photon tagging technique. We report for the first time an experimental signature for these effects.

Future work will include:

- Absolute energy calibration of the photon tagger.
- Quantification of the impact of limitations on the photon tagging technique for PrimEx experiment.
- More (parasitic) data collection in future runs.

## Bibliography

- [1] PrimEx Proposal, December 17, 1998.
- [2] D. I. Sober, H Crannell and F.J. Klein, CLAS-NOTE 2004-019, “The tagger energy scale: Interpreting the CMU Kinematic fit results.”
- [3] S. Stepanyan, B. Mecking, S. Boyarinov, H. Egiyan, L. Guo, D. Dale, M. Gabrielyan, L. Gan, A. Gasparyan, A. Teymurazyan, I. Nakagawa, A. Glamazdin, M. Wood, “Energy Calibration of the JLab Tagging System.”. Submitted to NIM.
- [4] D. I. Sober et al., “The bremsstrahlung tagged photon beam in Hall B at JLab”, Nucl. Instr. and Meth. A440, 263 (2000)
- [5] PrimEx CDR, March 3, 2000.
- [6] A. Gil, E. Oset, “Incoherent bremsstrahlung in nuclei”, Nuclear Physics A580 (1994), 517-537
- [7] GEANT-Detector Description and Simulation Tool, user’s manual. CERN Geneva, Switzerland, March 1994.
- [8] K. Mork and H. Olsen, Phys. Rev. 140, B1661 (1965)
- [9] H. D. Schulz and G. Lutz, Phys. Rev. 167, 1280 (1968)
- [10] M. Gabrielyan, Bulletin of the APS April Meeting 2006, Dallas, TX. Session B8.

## **Vita of Marianna Gabrielyan**

**DOB:** December 27, 1978

**Place of Birth:** Yerevan, ARMENIA.

### **Education**

B. S. in Physics, Yerevan State University, Armenia, 2000.

### **Positions**

2002 – 06 Research Assistant, Department of Physics and Astronomy,  
University of Kentucky

2002-06 Full time graduate student at the Department of Physics and Astronomy,  
University of Kentucky, specializing in experimental intermediate energy physics.

2000-01 Full time graduate student at the Department of Physics, Yerevan State  
University, specializing in experimental nuclear physics.

1996-2000 Full time undergraduate student at the Department of Physics, Yerevan State  
University (Armenia).

### **Awards, Honors and Professional Society Memberships**

Academic Excellency Award, Yerevan State University, 1999.

Member of American Physical Society

### **Abstracts and Publications**

1. S. Stepanyan, B. Mecking, S. Boyarinov, H. Egiyan, L. Guo, D. Dale, M. Gabrielyan, L. Gan, A. Gasparyan, A. Teymurazyan, I. Nakagawa, A. Glamazdin, M. Wood, “Energy Calibration of the JLab Tagging System.”. Submitted to NIM.
2. M. Gabrielyan, “Investigation of Limitations of the Photon Tagging Technique at High Energies”, Bulletin of the APS April Meeting 2006, Dallas, TX. Session B8.